Please cite this article in press as: Shi et al., Shugoshin 2A stabilizes heterochromatin complexes to suppress the 2-cell-like state in embryonic stem cells, Stem Cell Reports (2026), https://doi.org/10.1016/j.stemcr.2026.102824

STEM CELL REPORTS
Article
ISSCR
OPEN ACCESS

Shugoshin 2A stabilizes heterochromatin complexes to suppress the 2-cell-like state in embryonic stem cells

Panpan Shi,[1,2,5] Kairang Jin,[1,2,5] Guoxing Yin,[1,2,5] and Lin Liu[1,2,3,4,6,*]
[1]State Key Laboratory of Medicinal Chemical Biology, Nankai University, Tianjin 300350, China
[2]Frontiers Science Center for Cell Responses, College of Life Sciences, Nankai University, Tianjin 300071, China
[3]Tianjin Union Medical Center, Nankai University, Tianjin 300000, China
[4]Haihe Laboratory of Cell Ecosystem, Tianjin 300020, China
[5]These authors contributed equally
[6]Lead contact
*Correspondence: liulin@nankai.edu.cn
https://doi.org/10.1016/j.stemcr.2026.102824

SUMMARY

Two-cell (2C)-specific transcripts important for maternal zygotic transition, such as *Zscan4* and endogenous retrovirus (*MERVL*), are sporadically expressed in approximately 1%–5% of an embryonic stem cell (ESC) population to maintain ESC and telomere homeostasis. However, the molecular mechanisms regulating the 2-cell-like state in ESCs are not fully understood. Here, we show that *Sgo2a* is an important suppressor of the 2-cell-like state and telomere length. Loss of *Sgo2a* reduces the enrichment of heterochromatic H3K9me3 on 2C genes, including *Dux*, *Zscan4* gene clusters and downstream enhancers, resulting in activation of a 2-cell-like state. However, chromosome breakage was detected in *Sgo2a*-deficient ESCs. Mechanistically, SGO2A promotes the interaction between RIF1 and KAP1, regulates KAP1 ubiquitination, and maintains KAP1 stability at heterochromatin, repressing 2-cell genes. These results reveal a critical role for *Sgo2a* in suppressing the 2C-like state to maintain the homeostasis and genome stability of ESCs.

INTRODUCTION

Zygotic genome activation (ZGA) for the maternal-zygotic transition is essential for mammalian embryo development. ZGA occurs at the late 1- and 2-cell stages during early embryo development in mice and is regulated by epigenetic remodeling and transcription factors (Eckersley-Maslin et al., 2018; Jukam et al., 2017; Wu et al., 2016; Xu and Xie, 2018; Xu et al., 2021). The 2C-specific markers *Zscan4* and endogenous retrovirus (*MERVL*) are expressed sporadically in approximately 1%–5% of an embryonic stem cell (ESC) population (Falco et al., 2007; Macfarlan et al., 2012; Zalzman et al., 2010). Early 2C embryos and 2C-like cells display similar transcriptomes, chromatin accessibility landscapes, and regulatory architectures (Baker and Pera, 2018; Hendrickson et al., 2017; Macfarlan et al., 2012; Peaston et al., 2004; Rodriguez-Terrones et al., 2018; Wu et al., 2016). 2C-like cells can be a good model for understanding ZGA and totipotency. Many factors, such as DUX (De Iaco et al., 2017; Grow et al., 2021; Hendrickson et al., 2017; Whiddon et al., 2017), USP17L (Shi et al., 2025), ZSCAN4 (Yang et al., 2024; Zhang et al., 2019), DPPA2 and DPPA4 (De Iaco et al., 2019; Eckersley-Maslin et al., 2019; Yan et al., 2019), NELFA (Hu et al., 2020), and rRNA biogenesis (Yu et al., 2021), have been found to activate the transcription of the 2C-like state or ZGA. In contrast, heterochromatin and modifiers, including KAP1 (De Iaco et al., 2017; Percharde et al., 2018), RIF1 (Dan et al., 2014; Yoshizawa-Sugata et al., 2021), HP1 (Maksakova et al., 2013), H3K9me3 (Dan et al., 2014; Le et al., 2021), and modifiers (e.g., SETDB1 [Wu et al., 2020]), suppress the 2C-like state and ZGA, which is important for maintaining the homeostasis of ESCs and ZGA.

Shugoshin (SGO) is a conserved centromere protein that plays a crucial role in centromere cohesion and chromosome separation during mitosis and meiosis (Kawashima et al., 2007; Kerrebrock et al., 1995; Kitajima et al., 2004; Marston et al., 2004; Rabitsch et al., 2004; Salic et al., 2004; Tsukahara et al., 2010; Vanoosthuyse et al., 2007; Watanabe, 2005). SGO2 is essential for the formation of highly concentrated chromatin in the subtelomere region, repressing the transcription of subtelomeric genes in *Schizosaccharomyces pombe* (Kanoh, 2018). SGO2 preferentially localizes at subtelomeres during the G2 phase and is essential for the formation of a highly condensed subtelomeric chromatin body "knob." The absence of SGO2 leads to derepression of subtelomeric genes and premature DNA replication at subtelomeric late origins in the fission yeast *S. pombe* (Tashiro et al., 2016). In *S. pombe*, *Sgo2*-deficient cells exhibit changes in mitosis and meiosis, such as chromosomal bidirectional defects and sister chromatid unidirectional changes (Rabitsch et al., 2004; Vanoosthuyse et al., 2007; Vaur et al., 2005).

In mammals, SGO regulates cohesin, kinetochore-microtubule attachments, and chromosomal instability during meiosis (Sun et al., 2022). SGO2 is necessary to

Please cite this article in press as: Shi et al., Shugoshin 2A stabilizes heterochromatin complexes to suppress the 2-cell-like state in embryonic stem cells, Stem Cell Reports (2026), https://doi.org/10.1016/j.stemcr.2026.102824

protect centromere cohesion during meiosis I in mice but is not essential for mitosis (Llano et al., 2008). Centromeric cohesins at meiosis I are protected by SGO2 from separating-enzyme-mediated division, ensuring that sister chromatids remain together until they separate in meiosis II (El Yakoubi et al., 2017). Without SGO2, tension attachments cannot be established during metaphase of meiosis II and sister chromatids are randomly separated (Llano et al., 2008). In human oocytes, impaired SGO2 localization also weakens cohesion integrity and may lead to the increased incidence of aneuploidy observed in human oocytes with advanced maternal age (Mihalas et al., 2024). Additionally, SGO2 is an emerging differentially expressed molecule that can regulate RAB1A expression by inhibiting its ubiquitination during tumorigenesis (Lv et al., 2022). Here, we report critical functions of SGO2A in regulating the transcription of the 2C state and maintaining chromosome stability in mouse ESCs.

RESULTS

Sgo2a is dynamically distributed in mESCs

Sgo2a is an inhibitor of gene replication and transcription (Tashiro et al., 2016). Sequencing data from early embryos revealed that the *Sgo2a* transcript level rapidly decreased at the 2-cell stage (Figure S1A) (Zhou et al., 2021), especially at the early 2-cell stage (Figure S1B) (Zhang et al., 2016). In the translation landscape revealed by Ribo-seq (Ribosome profiling sequencing), the expression level of SGO2A in early 2-cell-stage embryos is also significantly decreased (Figure S1C) (Xiong et al., 2022). Minor ZGA in mice occurs from the S phase of the zygote to the G1 phase of the 2C embryo (Abe et al., 2018; Zhang et al., 2020). The 2C-like cells that express typical genes in 2C embryos, such as *Zscan4* and *MERVLs*, are found in approximately 1%–5% of an ESC population (Falco et al., 2007; Macfarlan et al., 2012; Zalzman et al., 2010). To explore the potential functions of *Sgo2a* in 2C-like cells, we sorted *Zscan4*-positive (*Zscan4*$^+$) and *Zscan4*-negative (*Zscan4*$^-$) ESCs via flow cytometry of tdTomato-*Zscan4* ESCs (Figures 1A and 1B) but did not detect differences in the RNA expression levels of *Sgo2a* in *Zscan4*$^+$ and *Zscan4*$^-$ ESCs (Figure 1C), which is consistent with the analysis of published data (Figure S1D) (Akiyama et al., 2015; Hormoz et al., 2016). However, the expression of the SGO2A protein was dynamic and negatively correlated with ZSCAN4 protein levels in *Zscan4*-marked cells (Figure 1D) (Zhang et al., 2016). By observing the localization of SGO2A in ESCs, we found that some SGO2A proteins seem to be localized on heterochromatin at interphase in ESCs (Figure 1E) and partly colocalized with telomere restriction fragment 1 (TRF1), which is indicative of telomere localization (Figure 1F). In dividing cells at mitosis, SGO2A was located at the end of the chromosome (Figure 1E) and strongly colocalized with TRF1 (Figure 1F), suggesting that SGO2A may be involved in telomere regulation. To explore the potential functions of *Sgo2a* in mESCs, we performed gene knockout experiments. The gene editing strategy was to delete the exon located at positions 17,555–17,640 of the genome (Figure S1E). After clone screening (Figure S1F), gene sequencing comparison (Figure S1G), and western blot detection (Figure S1H), *Sgo2a* was successfully knocked out.

Sgo2a deficiency affects multiple biological processes

After the *Sgo2a* gene was knocked out, the size of cell clones became smaller (Figure S2A), and the cell cycle slightly changed (Figure S2B). We performed RNA sequencing (RNA-seq) of *Sgo2a*-knockout ESCs compared with wild-type (WT) ESCs and obtained reliable results, with robust repeatability (Figure S2C). Knockout of *Sgo2a* affected the expression of pluripotency genes *Oct4*, *Dppa2*, *Lin28a*, etc. (Figures S2D–S2F) and multiple functional processes (Figures S3A and S3B). *Sgo2a* deficiency did not affect the expression of key telomerase genes (*Terc* and *Tert*) (Figures S3C–S3E). Notably, however, telomeres were longer in *Sgo2a* knockout ESCs than in WT control ESCs, as measured by qPCR (Figure S4A) (Callicott and Womack, 2006), quantitative fluorescence *in situ* hybridization (Q-FISH) (Poon et al., 1999) (Figures S4B and S4C), or TRF (Figure S4D). Moreover, chromosome breakage and telomere loss were detected after *Sgo2a* was knocked out (Figure S4B, S4E, and S4F). These data suggest that *Sgo2a* promotes telomere stability through telomerase-independent pathways.

Sgo2a deficiency derepresses 2C genes

ZSCAN4, a key upstream factor that promotes the activation of 2C genes (Yang et al., 2024; Zhang et al., 2019), can extend telomeres through a telomerase-independent recombination mechanism and promote genomic stability (Zalzman et al., 2010). Therefore, we hypothesized that the knockout of *Sgo2a* might activate the *Zscan4* gene. The overall transcription levels of 2C genes, including *Dux*, *Zscan4*, *Usp17l*, and *Obox6* (Figure 2B), indeed increased in *Sgo2a* knockout ESCs (Figure 2A), and typical retrotransposons, including *MERVLs* (Figure 2C), were also upregulated. We further verified the upregulation of 2C genes after *Sgo2a* knockout via qPCR (Figure 2D) and western blot (Figure 2E). Furthermore, we knocked out *Sgo2a* in tdTomato-*Zscan4* ESCs (Figures S5A–S5C). Consistent results revealed that

Please cite this article in press as: Shi et al., Shugoshin 2A stabilizes heterochromatin complexes to suppress the 2-cell-like state in embryonic stem cells, Stem Cell Reports (2026), https://doi.org/10.1016/j.stemcr.2026.102824

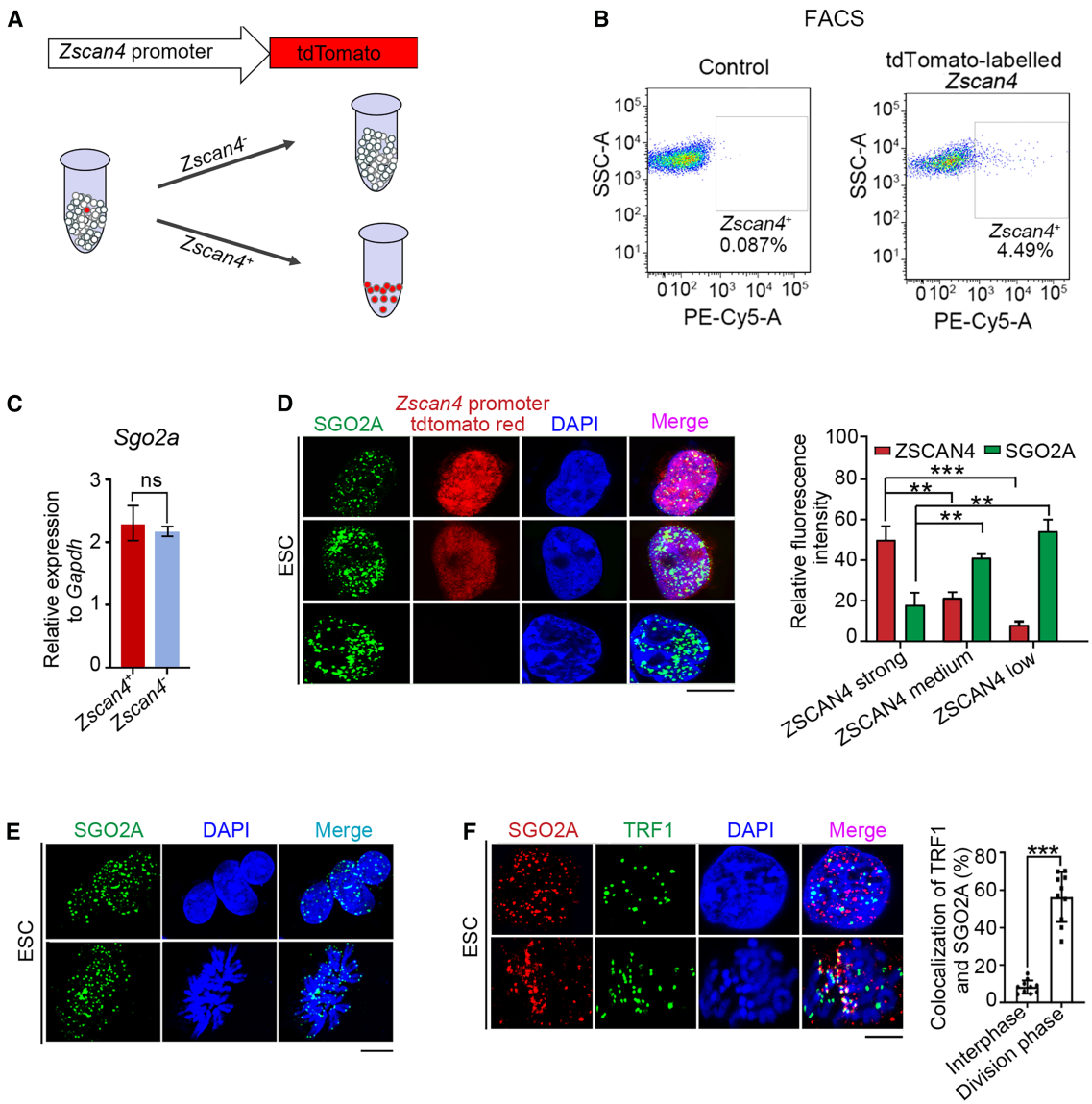

Figure 1. *Sgo2a* is dynamically expressed in mESCs

(A) Sorting diagram of *Zscan4*-positive cells. tdTomato-labeled *Zscan4*$^+$ cells.

(B) Flow cytometry sorting of *Zscan4*$^+$ and *Zscan4*$^-$ ESCs based on tdTomato in control and tdTomato-labeled *Zscan4*-expressing ESCs.

(C) Expression levels of *Sgo2a* mRNA determined by qPCR, with *Zscan4*$^-$ ESCs serving as controls. *Zscan4*$^+$ and *Zscan4*$^-$ ESCs were sorted via flow cytometry (n = 3 independent experiments). The data are shown as the means ± SDs (two-tailed Student's t test).

(D) Immunofluorescence of SGO2A in ESCs. SGO2A (green) was revealed by a specific antibody, and ZSCAN4 was revealed by red fluorescence. Scale bar, 10 μm. (Right) Fluorescence statistics of ZSCAN4 and SGO2A. The fluorescence intensity of ZSCAN4 was divided into three grades: strong, medium, and low, and the corresponding fluorescence intensity of SGO2A was calculated (n = 3 independent experiments). The data are shown as the means ± SDs (two-tailed Student's t test); $^{**}p < 0.01$, $^{***}p < 0.001$.

(E) Immunofluorescence of SGO2A in ESCs at interphase and during division. SGO2A (green) was revealed by a specific antibody, and the DNA was stained with DAPI. Scale bar, 10 μm.

(F) Co-immunostaining and fluorescence microscopy for SGO2A (red) and TRF1 (green) in ESCs. DNA was stained with DAPI. Scale bar, 10 μm. (Right) SGO2A and TRF1 immunofluorescence colocalization statistics (n = 3 independent experiments). The data are shown as the means ± SDs (two-tailed Student's t test); $^{***}p < 0.001$.

Please cite this article in press as: Shi et al., Shugoshin 2A stabilizes heterochromatin complexes to suppress the 2-cell-like state in embryonic stem cells, Stem Cell Reports (2026), https://doi.org/10.1016/j.stemcr.2026.102824

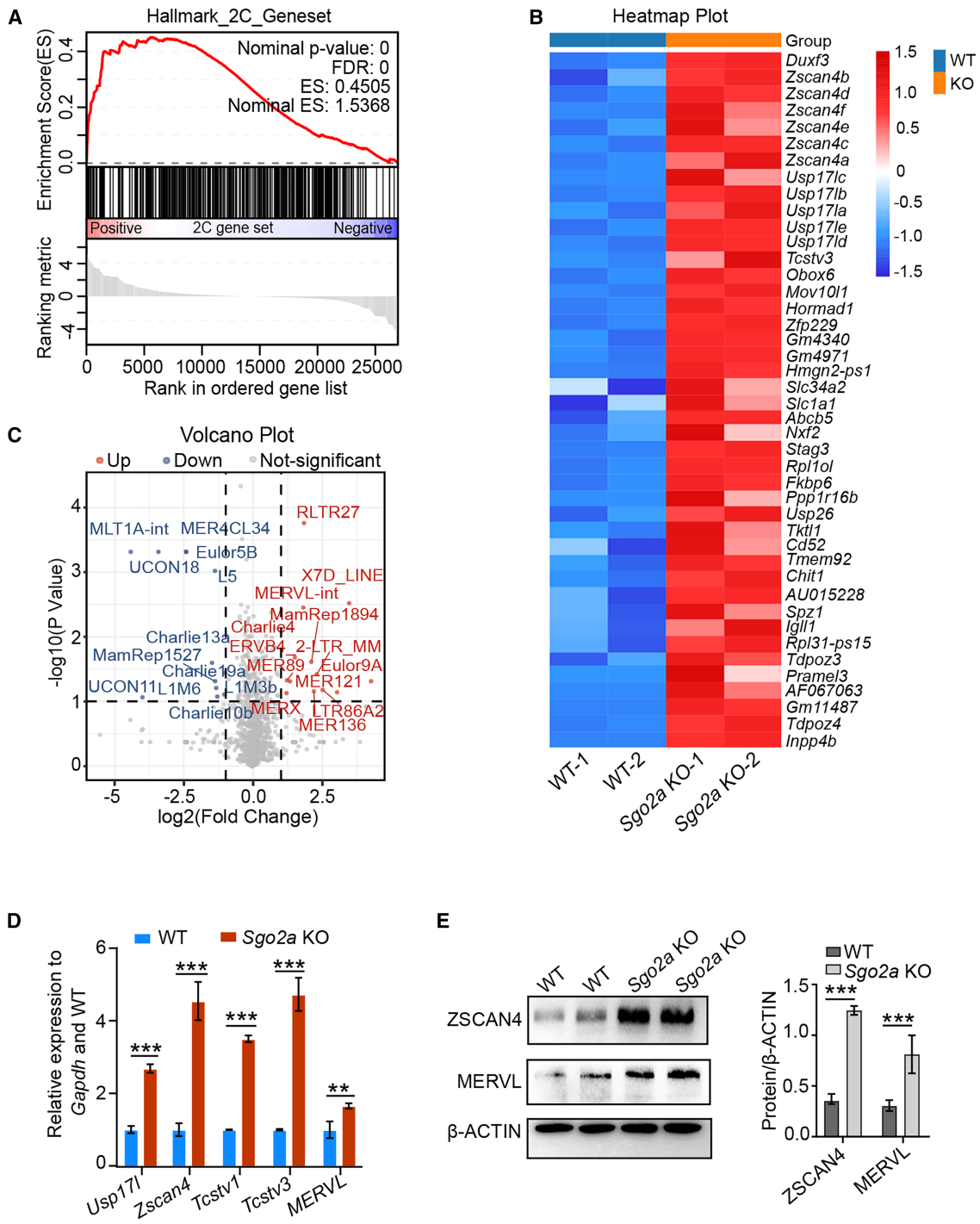

Figure 2. *Sgo2a* deficiency derepresses 2C genes

(A) Gene set enrichment analysis (GSEA) revealed that upregulated genes were highly enriched in the 2C gene set by RNA sequencing after *Sgo2a* knockout. WT served as a control.

(B) Heatmap of 2C genes after *Sgo2a* knockout. The colors from blue to red in ascending order represent gene expression from low to high.

(C) Changes in the expression of retrotransposons, including *MERVs,* as determined via RNA-seq analysis following *Sgo2a* knockout.

(legend continued on next page)

ZSCAN4 was upregulated significantly (Figure S5D), and flow cytometry analysis revealed a significant increase in the proportion of *Zscan4*$^+$ cells (Figure S5E). These results suggest that *Sgo2a* is an important suppressor of 2C genes.

SGO2A suppresses 2C genes by regulating H3K9me3 enrichment

Furthermore, *Sgo2a* knockout reduced the number of large bright foci of condensed heterochromatin in ESCs (Figure 3A). We examined the levels of heterochromatin-associated histone modifications via western blotting and revealed that H3K9me3 protein levels were noticeably reduced in *Sgo2a*-deficient ESCs (Figure 3B). Immunofluorescence microscopy confirmed that H3K9me3 levels and heterochromatin foci were similarly reduced, as determined by DAPI staining (Figure 3C). Moreover, the coimmunoprecipitation (Co-IP) results indicated that SGO2A interacted with H3K9me3 (Figure 3D).

We speculated that SGO2A might affect the transcription of 2C genes through regulating H3K9me3 and heterochromatin organization. To test this hypothesis, CUT&Tag experiments for H3K9me3 were performed in WT ESCs compared with *Sgo2a*-deficient ESCs. Consistent with the results of western blot (Figure 3B), the enrichment of H3K9me3 on the genome was reduced due to the knockout of *Sgo2a* (Figure S6A). The knockout of *Sgo2a* alters the enrichment of H3K9me3 on the 2C genes (Figure 3E). Similarly, it also significantly influences the signal intensity of H3K9me3 on LTR (Li et al., 2023) (Figure S6B), *ERVs* (Fueyo et al., 2022; Macfarlan et al., 2012; Rowe et al., 2013) (Figures S6C and S6D), and special sequences (Walsh et al., 1998) (Figure S6E) near the genes. Although the binding to the special sequences such as the downstream poly-cytosine of *Rps9* may be unstable (Figure S6F [Barral et al., 2022; Zhang et al., 2024] and Figure S6G [Enriquez-Gasca et al., 2023; Gaurav et al., 2025; Palma et al., 2025; Pinzon-Arteaga et al., 2024; Spencley et al., 2023; Wen et al., 2023]), this might precisely be the most genuine manifestation of the heterogeneity and dynamics of H3K9me3 in mESCs. The strong H3K9me3 signal on *Dux* decreased sharply in *Sgo2a*-deficient ESCs (Figure 3F). A previous study showed that the activation of 2C genes is related to the altered enrichment of H3K9me3 in the *Zscan4* gene cluster and downstream enhancers (Figure S6H) (Le et al., 2021). On the basis of chromatin interaction data from 2-cell embryos, enhancers located downstream of the ~ 2-Mb region of the *Zscan4* gene play a significant role in the activation of *Zscan4* (Le et al., 2021). Our CUT&Tag data demonstrated that knockout of *Sgo2a* in ESCs actually reduced the enrichment of H3K9me3 on the *Zscan4* gene cluster and the enhancer (Figure 3G).

SGO2A regulates the ubiquitination of KAP1

To explore how SGO2A regulates H3K9me3, we analyzed the transcriptome of the H3K9 methylation complex or modifiers via RNA-seq (Dan et al., 2014). No significant changes in the number of members of the complex were detected in *Sgo2a*-deficient ESCs (Figures S6I and S6J). However, the protein level of KAP1, which maintains the H3K9 methylation complex, was decreased in *Sgo2a* knockout ESCs (Figure 4A). Moreover, overexpression of KAP1 in *Sgo2a* knockout ESCs rescued the loss of H3K9me3 (Figure 4B). These results suggest that decreased KAP1 protein levels could be involved in the decrease in H3K9me3 in *Sgo2a*-knockout ESCs. Next, we tested how SGO2A regulates KAP1 protein levels. Inhibition of protein synthesis by cycloheximide (CHX) demonstrated that KAP1 degradation occurred only slightly in WT cells, which is consistent with the results of previous studies (Le et al., 2021). However, loss of *Sgo2a* accelerated KAP1 degradation (Figure 4C). Given that KAP1 can be regulated by ubiquitination (Le et al., 2021), we used MG132 to inhibit the degradation of ubiquitinated proteins. KAP1 exhibited more obvious accumulation in *Sgo2a*-deficient ESCs than in WT ESCs treated with MG132 (Figure 4D), indicating that the low levels of KAP1 induced by *Sgo2a* deficiency are caused by ubiquitination. The subsequent ubiquitination experiment again verified that SGO2A deficiency led to increased ubiquitination of KAP1 (Figure 4E). Moreover, Co-IP experiments demonstrated the interaction of these two proteins (Figure 4F). Therefore, SGO2A stabilizes the KAP1 protein via deubiquitination.

The reduction in H3K9me3 caused by KAP1 degradation is the key mechanism by which SGO2A regulates 2C genes

KAP1 is involved in heterochromatin maintenance and the inhibition of 2C genes, including *Zscan4,* in ESCs (Maksakova et al., 2013). KAP1 can also exert transcriptional inhibition by maintaining H3K9me3 marks at enhancers (Rowe et al., 2013). Recently, KAP1 was shown to regulate the enrichment of H3K9me3 on the *Zscan4* gene cluster and downstream enhancers (Le et al., 2021). These

(D) qPCR results showing the changes in 2C genes after *Sgo2a* knockout (n = 3 independent experiments). The data are shown as the means ± SDs (two-tailed Student's t test); $^{**}p < 0.01$, $^{***}p < 0.001$.

(E) Western blot showing the changes in ZSCAN4 and MERVL after *Sgo2a* knockout. The right graph shows the quantification of ZSCAN4 and MERVL compared with β-ACTIN (n = 3 independent experiments). The data are shown as the means ± SDs (two-tailed Student's t test); $^{***}p < 0.001$.

Please cite this article in press as: Shi et al., Shugoshin 2A stabilizes heterochromatin complexes to suppress the 2-cell-like state in embryonic stem cells, Stem Cell Reports (2026), https://doi.org/10.1016/j.stemcr.2026.102824

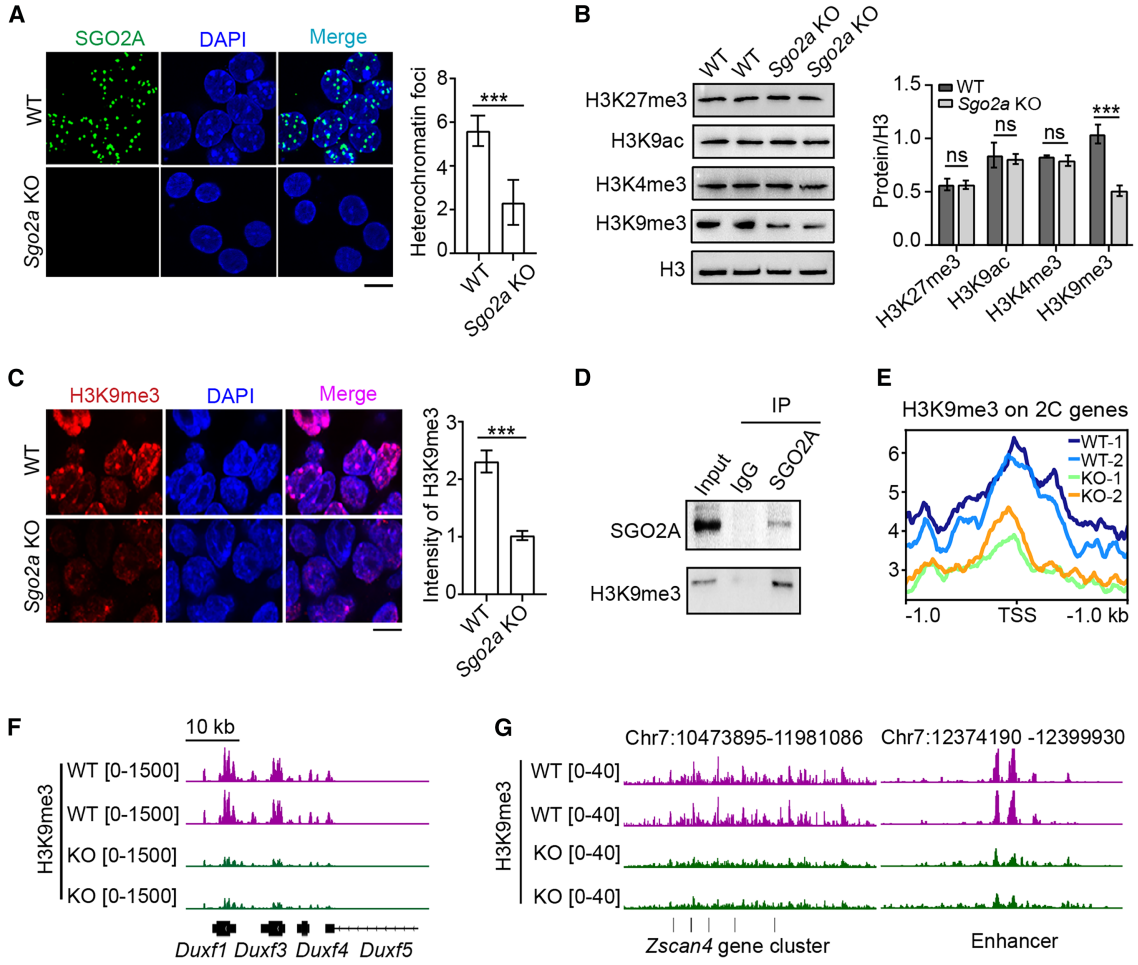

Figure 3. SGO2A regulates the enrichment of H3K9me3 on *Dux*, the *Zscan4* gene cluster, and downstream enhancers

(A) Immunofluorescence of SGO2A in WT and *Sgo2a*-deficient ESCs. Scale bar, 10 μm. (Right) Statistics of heterochromatin foci (n = 3 independent experiments).

(B) Western blot showing the changes in histone modification after *Sgo2a* knockout. The right graph shows the quantification of histone modifications compared with H3 (n = 3 independent experiments). ns, not significant; ***p < 0.001.

(C) Immunofluorescence of H3K9me3 in WT and *Sgo2a*-deficient ESCs. H3K9me3 (red) was revealed by a specific antibody, and the DNA was stained with DAPI. Scale bar, 10 μm. (Right) Fluorescence statistics of H3K9me3 (n = 3 independent experiments).

(D) CoIP verified the interaction of SGO2A with H3K9me3. IgG served as a negative control.

(E) CUT&Tag data displaying H3K9me3 enrichment on the whole 2C gene on the basis of the mm10 mouse genome after *Sgo2a* knockout.

(F) IGV plot displaying H3K9me3 enrichment on the *Dux* gene cluster on the basis of the mm10 mouse genome in WT and *Sgo2a*-deficient ESCs.

(G) IGV plot displaying the enrichment of H3K9me3 on *Zscan4* gene cluster and the downstream enhancer. The location of the enhancer refers to the published data from Rongrong Le et al., *Cell Stem Cell* 2021.

findings indicate that KAP1 plays a significant role in the regulation of 2C genes. *Kap1* overexpression in *Sgo2a*-deficient ESCs abrogated the increased expression of 2C genes, further demonstrating that KAP1 is a key intermediate factor in the regulation of 2C genes by *Sgo2a* (Figures 5A and 5B).

To further investigate how KAP1 regulates 2C genes in *Sgo2a*-deficient ESCs, we conducted CUT&Tag analysis. The enrichment of KAP1 in the genome was significantly reduced in *Sgo2a*-deficient ESCs (Figure 5C), which was consistent with the western blot results (Figure 4A). The signal of KAP1 on the 2C genes also showed a significant decrease after *Sgo2a* knockout (Figure 5D), suggesting a regulatory effect on the 2C genes. Specifically, similar to H3K9me3, KAP1 was strongly enriched on *Dux*, and its enrichment was reduced due to the knockout of *Sgo2a*. (Figure 5E). Unlike specific binding at *Dux*, KAP1 shows a weaker signal at *Zscan4* (Figure 5F) (Le et al., 2021). However,

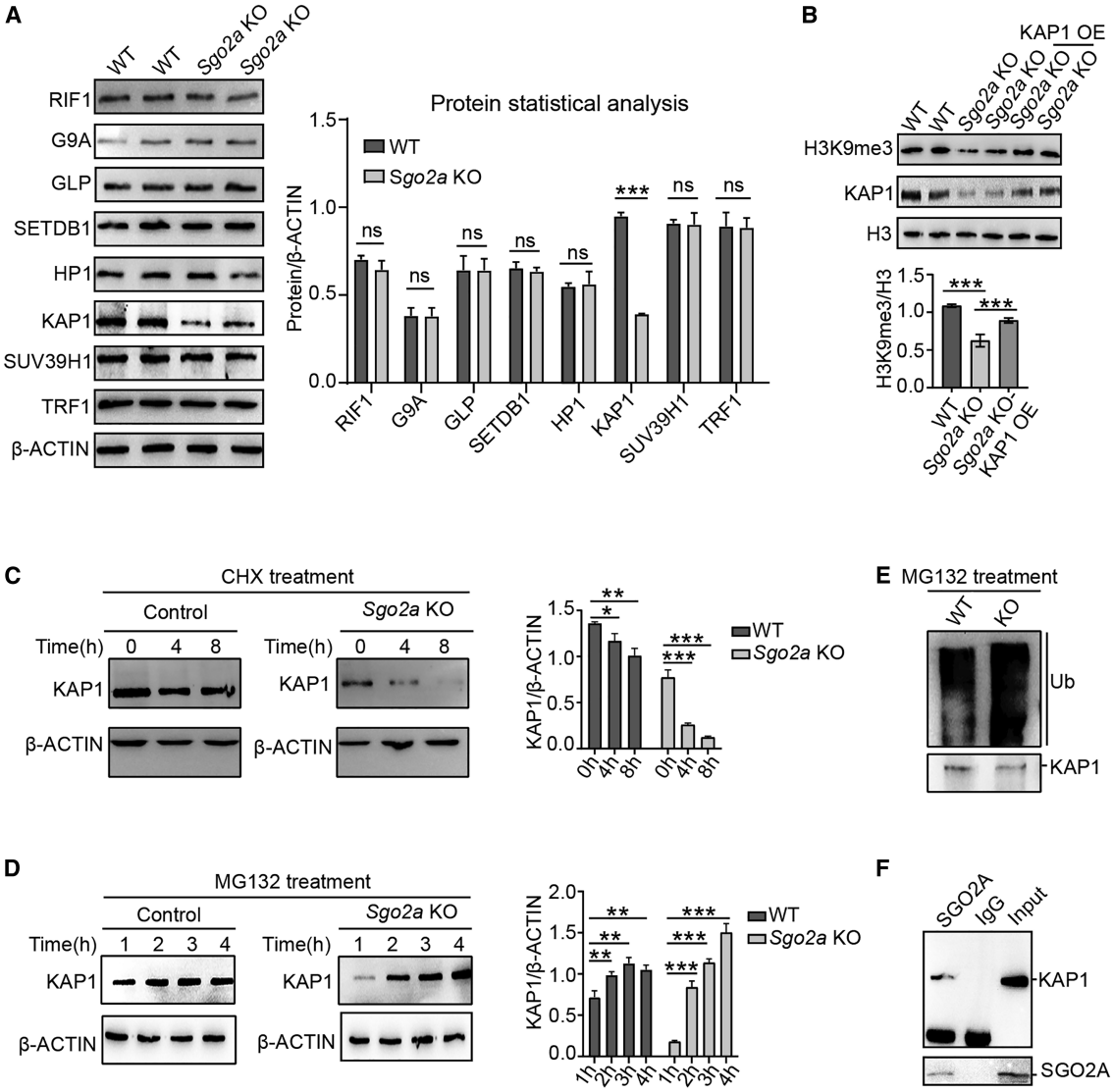

Figure 4. SGO2A regulates the stability of the heterochromatin complex component KAP1

(A) Western blot showing changes in heterochromatin complex member protein levels after *Sgo2a* knockout. The right graph shows the quantification of heterochromatin complex members compared with β-ACTIN (n = 3 independent experiments).

(B) Western blot showing the level of H3K9me3 in the WT, *Sgo2a* knockout (KO), and *Sgo2a* KO-*Kap1* OE cell lines. *Sgo2a* KO-*Kap1* OE refers to the overexpression of *Kap1* in *Sgo2a* KO cell lines. The right graph shows the quantification of H3K9me3 compared with H3 (n = 3 independent experiments).

(C) Western blot analysis revealed that *Sgo2a* knockout accelerated the degradation of KAP1. CHX was added at 20 mg/mL, and samples were collected every 4 h. Right graph showing the quantification of the expression of the heterochromatin complex member KAP1 compared with that of β-ACTIN (n = 3 independent experiments).

(D) Accumulation of KAP1 by treatment with MG132, as detected by western blotting. MG132 was added at 10 μM, and samples were collected every 1 h. (Right) Quantification of the expression of the heterochromatin complex member KAP1 compared with that of β-ACTIN (n = 3 independent experiments).

(E) Western blot showing the ubiquitination level of KAP1 in the WT and *Sgo2a*-KO cell lines.

(F) CoIP experiments validating the interaction of SGO2A with KAP1. IgG served as a negative control.

The statistical data are shown as the means ± SDs (two-tailed Student's t test); $^{*}p < 0.05$, $^{**}p < 0.01$, $^{***}p < 0.001$.

Please cite this article in press as: Shi et al., Shugoshin 2A stabilizes heterochromatin complexes to suppress the 2-cell-like state in embryonic stem cells, Stem Cell Reports (2026), https://doi.org/10.1016/j.stemcr.2026.102824

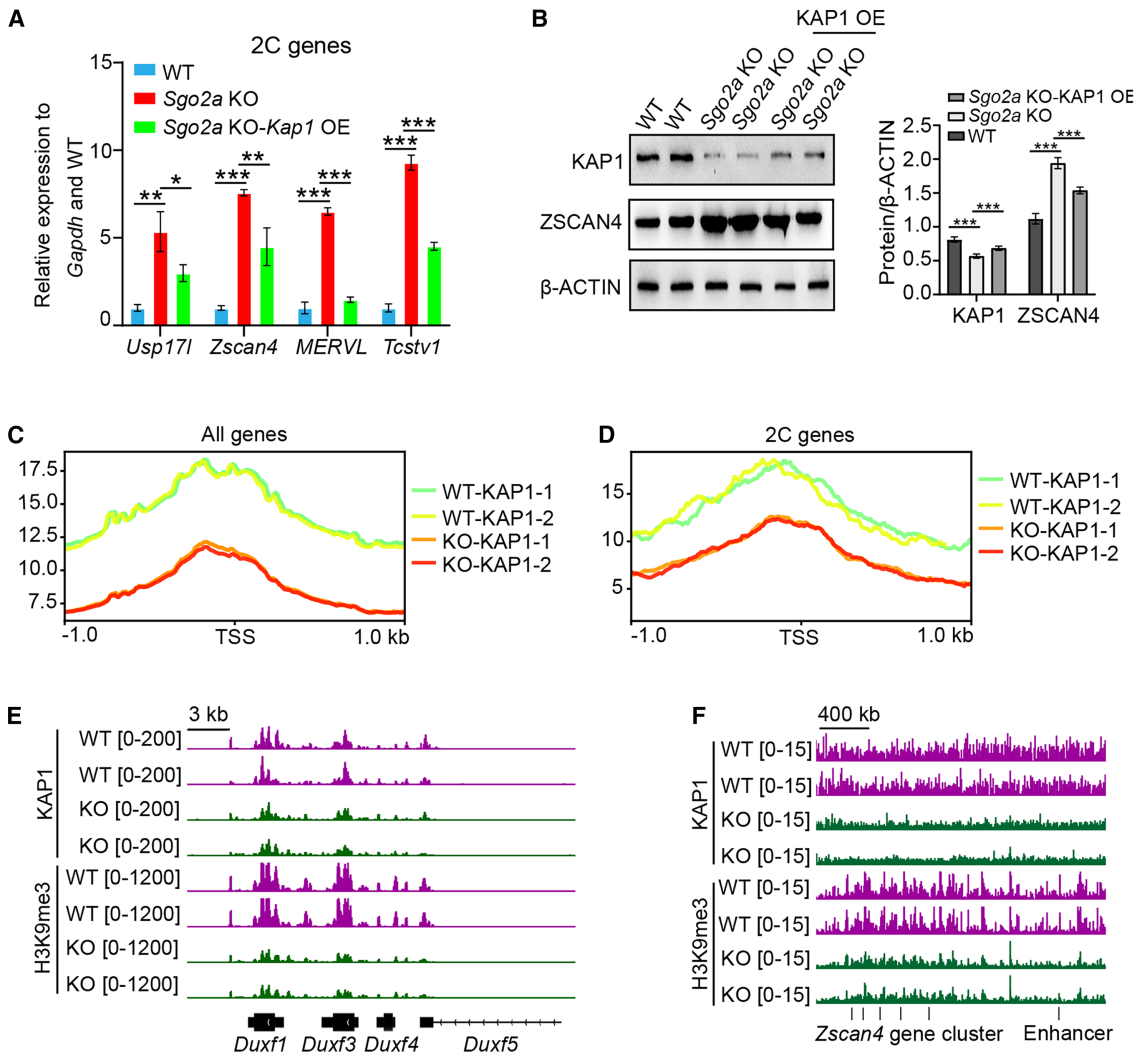

Figure 5. KAP1 is an important intermediate regulatory factor for SGO2A in the regulation of 2C genes

(A) qPCR results showing the transcription levels of 2C genes in the WT, *Sgo2a* knockout (KO), and *Sgo2a* KO-*Kap1* OE cell lines. *Sgo2a* KO-*Kap1* OE refers to the overexpression of *Kap1* in *Sgo2a* KO cell lines ($n = 3$ independent experiments). The data are shown as the means ± SDs (two-tailed Student's *t* test); $*p < 0.05$, $**p < 0.01$, $***p < 0.001$.

(B) Western blot showing the protein level of ZSCAN4 in the WT, *Sgo2a* KO, and *Sgo2a* KO-*Kap1* OE cell lines. *Sgo2a* KO-*Kap1* OE refers to the overexpression of *Kap1* in *Sgo2a* KO cell lines. The right graph shows KAP1 and ZSCAN4 compared with ACTIN ($n = 3$ independent experiments). The data are shown as the means ± SDs (two-tailed Student's *t* test); $***p < 0.001$.

(C) CUT&Tag data displaying KAP1 enrichment on whole genes on the basis of the mm10 mouse genome in WT and *Sgo2a*-deficient ESCs.

(D) IGV plot displaying KAP1 enrichment on 2-cell genes on the basis of the mm10 mouse genome in WT and *Sgo2a*-deficient ESCs.

(E) IGV plot displaying KAP1 and H3K9me3 enrichment on *Dux* on the basis of the mm10 mouse genome in WT and *Sgo2a*-deficient ESCs.

(F) IGV plot displaying the enrichment of KAP1 and H3K9me3 on the *Zscan4* gene cluster and downstream enhancers.

the decrease in H3K9me3 at *Zscan4* resulting from KAP1 degradation serves as a powerful impetus for the burst of *Zscan4* and its downstream enhancers (Figure 5F) (Le et al., 2021). The activation of *Zscan4* further mediates the opening of heterochromatin, promoting the transcription of 2C genes (Yang et al., 2024). The reinforcing feedback loop between 2C genes (e.g., *Dux* and *Usp17l* [Shi et al., 2025]) and *Zscan4* drives a transcriptional burst of 2C genes.

SGO2A strengthens the interaction between KAP1 and RIF1

SGO2A has also been shown to prevent ubiquitination degradation to maintain substrate stability in cancer cells (Lv et al., 2022). Additionally, KAP1 is protected by RIF1 in ESC cells (Dan et al., 2014). We asked whether this protection is broken by the absence of SGO2A. Our data revealed that SGO2A interacted with both KAP1 (Figure 6A)

Please cite this article in press as: Shi et al., Shugoshin 2A stabilizes heterochromatin complexes to suppress the 2-cell-like state in embryonic stem cells, Stem Cell Reports (2026), https://doi.org/10.1016/j.stemcr.2026.102824

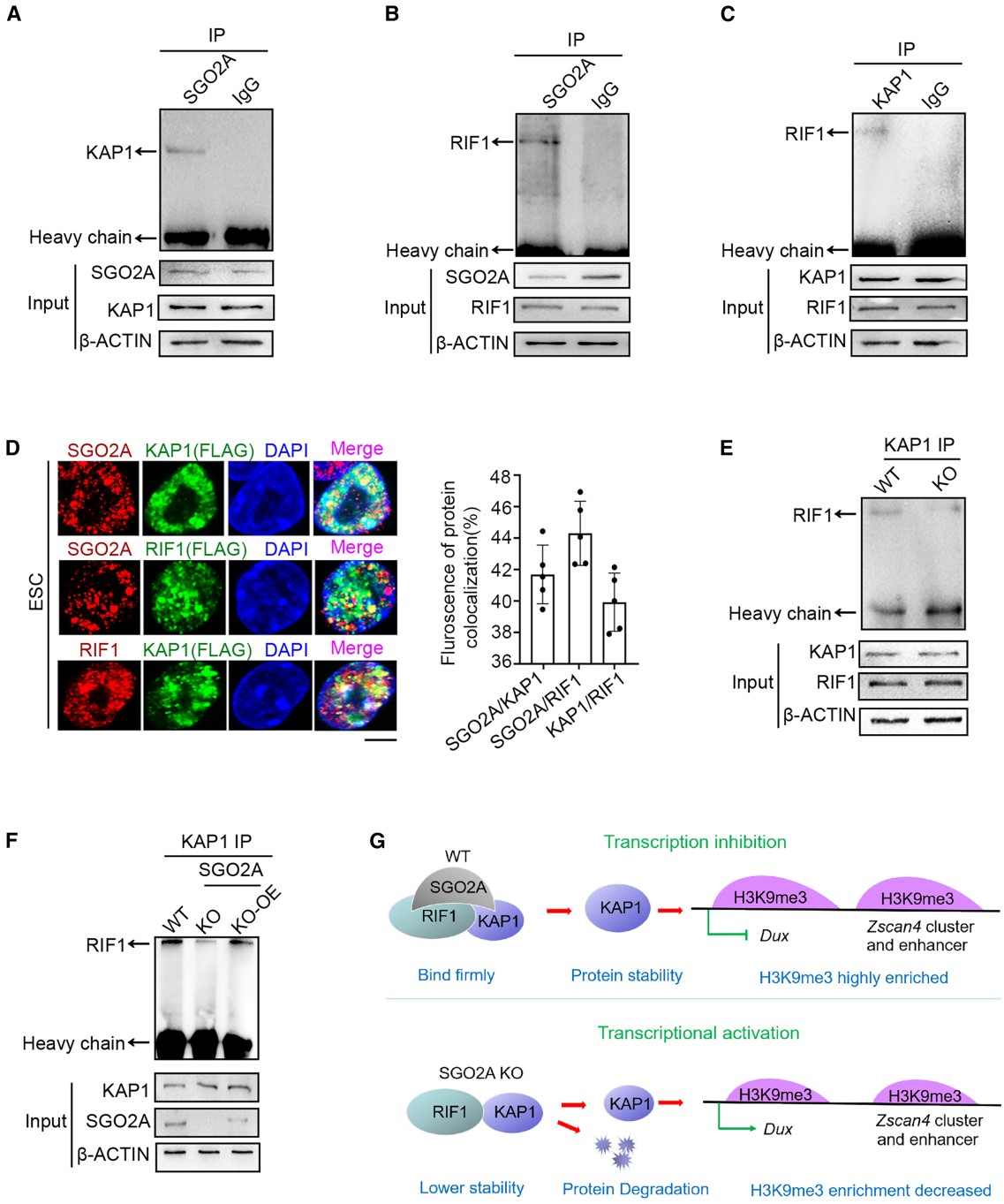

Figure 6. SGO2A promotes the interaction between KAP1 and RIF1

(A and B) Co-IP experiments validating the interaction of SGO2A with KAP1 (A) and RIF1 (B).

(C) Co-IP experiments validating the interaction of KAP1 with RIF1. IgG served as a negative control.

(D) Immunofluorescence was used to verify the colocalization of SGO2A, KAP1, and RIF1; scale bar, 10 μm. (Right) Immunofluorescence colocalization statistics (n = 2 independent experiments).

(E) Co-IP experiments verified the interaction of KAP1 with RIF1 in the WT and *Sgo2a*-KO cell lines. The cells were treated with MG132 at a concentration of 10 μM for 3 h to ensure that the Kap1 protein levels in the WT and *Sgo2a* KO cell lines were consistent.

(legend continued on next page)

and RIF1 (Figure 6B). We also confirmed the interaction between KAP1 and RIF1 (Figure 6C). Immunofluorescence colocalization also suggested interactions among the three proteins (Figure 6D). Therefore, SGO2A, RIF1, and KAP1 can interact with each other, which could be critical for heterochromatin assembly and condensation in mouse ESCs.

We tested whether the absence of SGO2A abrogates the interaction between RIF1 and KAP1. We conducted Co-IP experiments using WT and *Sgo2a*-knockout cell lines. The interaction between RIF1 and KAP1 was weakened in *Sgo2a* knockout ESCs compared with WT ESCs (Figure 6E), and the interaction between RIF1 and KAP1 was restored by replenishment with SGO2A (Figure 6F). These results support the notion that SGO2A can enhance the interaction between RIF1 and KAP1, thus maintaining the stability of KAP1. In conclusion, SGO2A maintains KAP1 stability and enriches H3K9me3 on *Zscan4* gene clusters and downstream enhancers to suppress 2C genes (Figure 6G).

DISCUSSION

We identified a critical role for SGO2A in regulating the 2C state in mESCs. Moreover, SGO2A regulates the enrichment of H3K9me3 on *Dux*, the *Zscan4* gene cluster, and downstream enhancers, thus suppressing 2C genes in mESCs. This regulation is achieved by regulating KAP1 ubiquitination and interacting with RIF1. In ESCs, KAP1 acts primarily as a transcriptional suppressor (Rowe et al., 2013), which is involved in heterochromatin maintenance and the inhibition of 2C genes, including *Zscan4* (Dan et al., 2014; Maksakova et al., 2013). RIF1 inhibits the expression of *Zscan4* and *ERVs* by maintaining H3 lysine 9 trimethylation (H3K9me3) (Dan et al., 2014; Li et al., 2017; Yoshizawa-Sugata et al., 2021). The stable maintenance of the H3K9 methylation complex depends on RIF1 binding to important components of the methylation complex, including KAP1, SUV39H1, heterochromatin protein α, G9A, and GLP, to prevent their degradation (Dan et al., 2014). SGO2A plays an important role in enhancing the interaction of RIF1 and KAP1, thereby mediating heterochromatin maintenance and inhibition of the 2C state. Although we are not sure which E3 ligase is involved in this regulatory process, it is likely that SGO2A enables the RIF1 complex to bind tightly, spatially shield the ubiquitination sites of KAP1, and prevent E3 ubiquitin-protein ligases from binding to KAP1, thereby stabilizing KAP1. Multiple E3 ligases may be involved in the process by which SGO2A regulates the stability of KAP1. It is also possible that KAP1 undergoes self-regulation, which is worthy of further in-depth study or is a special topic for research. Further experiments are needed to test the potential underlying mechanisms in the future.

We observed that 2C genes located in the subtelomere region, such as the *Zscan4* gene cluster, *Tcstv3*, and some *ERVs* (endogenous retroviruses), were upregulated in *Sgo2a*-deleted ESCs. ZSCAN4 can regulate telomere elongation and genomic stability in ESCs (Zalzman et al., 2010). In addition, TRF1 (van Steensel and de Lange, 1997), KAP1 (Wang et al., 2021), and RIF1 (Dan et al., 2014) are involved in telomere regulation and SGO2A colocalizes with KAP1, RIF1, and TRF1, suggesting that SGO2A itself is an important factor in telomere regulation. The suppression of *Zscan4* by SGO2A may regulate telomere homeostasis. *Sgo2a* deficiency leads to chromosome breakage and thus genome instability.

qPCR data and public data both indicate that the transcriptional level of *Sgo2a* is not significantly different between *Zscan4*$^+$ and *Zscan4*$^-$ cells. However, the expression of the SGO2A protein was dynamic and negatively correlated with ZSCAN4 protein levels in *Zscan4*$^+$ cells (Figure 1D) (Zhang et al., 2016). Posttranslational modifications, such as ubiquitination, are likely involved. Although there are no current studies reporting the ubiquitination of SGO2A, through UbiBrowser 2.0 (Wang et al., 2022), a comprehensive database for proteome-wide known and predicted ubiquitin ligase/deubiquitinase-substrate interactions in eukaryotic species, we predicted five potential ubiquitin E3 ligases (FBXO5, FBXO43, BTRC, MARCHF5, and MARCHF7) for SGO2A, indicating that SGO2A may be subject to ubiquitination degradation under certain circumstances. This may alter SGO2A protein levels in heterogeneous ESCs, such that reduced SGO2A protein levels resulted in elevated expression of ZSCAN4 in approximately 1%–5% of ESCs, whereas the SGO2A protein level remained high in the majority of ESCs not in 2C state. There might be specific posttranslational modifications (Ciechanover et al., 1990; Cui et al., 2025; Min et al., 2010) that regulate the protein level of SGO2A or other

(F) The interaction between KAP1 and RIF1 was verified by Co-IP after SGO2A OE was replenished in *Sgo2a*-KO cell lines. The cells were treated with MG132 at a concentration of 10 μM for 3 h to ensure that the KAP1 protein levels in the WT and *Sgo2a* KO cell lines were consistent.

(G) Model map of *Sgo2a* regulation of the 2C genes: SGO2A can maintain KAP1 stability by enhancing the interaction between RIF1 and KAP1, thereby affecting the enrichment of H3K9me3 on *Zscan4* gene clusters and downstream enhancers to achieve regulation of the 2C genes.

posttranscriptional regulatory mechanisms (Aranega and Franco, 2024; Weber et al., 1989; Yamamoto et al., 2023), which warrants further investigation. The characteristics of the SGO2A expression pattern could underlie the molecular basis of the dynamic activation of 2C genes.

Limitations of the study

Our data reveal the molecular mechanism of SGO2A inhibition of 2C genes in ESCs. We show that SGO2A stabilizes the substrate KAP1 by enhancing the interaction between RIF1 and KAP1. We cannot rule out the possibility that SGO2A directly regulates KAP1 deubiquitination. Additionally, SGO2A has been shown to localize to centromeres. Here, we found that SGO2A can also colocalize with TRF1 at telomeres, and this colocalization differs between the interphase and division phase, suggesting its dynamic regulatory roles at telomeres. The underlying molecular mechanism remains to be further explored in the future.

METHODS

ES cell culture

E3 and J1 cell lines were used in this study. E3 ESCs were cultured on MEF feeder cells (Ye et al., 2021), whereas J1 ESCs were cultured on gelatin. The culture medium of ESCs consisted of 15% fetal bovine serum (ES quality, HyClone) supplemented with penicillin (100 U/mL) and streptomycin (100 μg/mL), LIF (1000 U/mL) (ESGRO, Chemicon), nonessential amino acids, β-mercaptoethanol (0.1 mM), L-glutamine (1 mM), and knockout DMEM (Gibco). ESCs were cultured in a sterile incubator at 37°C in 5% CO_2. The cells were stored in liquid nitrogen and rapidly thawed in a 37°C water bath for recovery. The cells were passaged every 2 days at a 1:8 ratio. The cells were in good condition without *Mycoplasma* or bacterial contamination.

Generation of knockout ESCs via sgRNA (single-guide RNA)

sgRNAs were designed for the *Sgo2a* knockout experiment via the online design sgRNA (https://www.zlab.bio/guide-design-resources). The sequences of the sgRNAs were as follows:

Sgo2a-sgRNA-F: CACCGAATACTTAGCTGGCATGAAC
Sgo2a-sgRNA-R: AAACGTTCATGCCAGCTAAGTATTC

Single-stranded sgRNA was annealed into double-stranded sgRNA, and a knockdown vector was subsequently constructed. The annealing procedure was 95°C for 30 s, 72°C for 2 min, 56°C for 2 min, 37°C for 2 min, 25°C for 2 min, and storage at 4°C. The resulting double-stranded DNA is subsequently inserted into the knockout vector. The plasmids were transfected into ESCs via the Lonza nuclear transfer apparatus. After 24 h, 1.5 μg/mL puromycin was added for screening, and the *Sgo2a* knockout cell clone was subsequently selected for culture identification. Stable *Sgo2a* knockout ESCs were then selected with 1.5 μg/mL puromycin for 1 week.

Gene expression detection

The primers were designed via Primer 5 software, where qPCR primers (Table S1) were used to detect changes in 2C genes. Trans1-T1 phage-resistant chemically competent cells (Trans, CT111-01) were used to express exogenous genes. Positive clones were screened by ampicillin and PCR. The Kap1 plasmid was provided by Yang Jiao in our laboratory. The plasmid was transfected into ESCs with Hieff Trans Liposomal Transfection Reagent (Yeasen, 40802ES02) according to the manufacturer's instructions. The RNA was extracted 48 h later via the RNeasy Plus Mini Kit (QIAGEN, 74134) for reverse-transcription PCR (RT-PCR) detection.

RT-qPCR

Total RNA was extracted with the RNeasy Plus Mini Kit (QIAGEN, 74134). The concentration of total RNA was determined with a NanoDrop 2000 (Thermo Scientific). 1 μg of RNA was reverse transcribed to cDNA via M-MLV reverse transcriptase (Thermo Scientific, 28025021). cDNA was subsequently quantified via a real-time PCR system (Life Technologies). The primers used for the qPCR analysis are listed in Table S1.

Co-IP

SGO2A antibody was added to the prepared sample, which was subsequently incubated overnight at 4°C with gentle agitation to form the immune complex. The antibody mixture (immune complex) was transferred to a tube containing the prewashed protein A agarose bead pellet and incubated for 3 h at 4°C with constant gentle agitation. The pelleted beads were separated by centrifugation, and the supernatant was discarded. The pellet was washed with 600 μL of cell lysis buffer three times and resuspended in 80 μL of SDS buffer, followed by pipetting up and down several times to mix the sample. The sample was boiled for 6 min, after which SDS-PAGE was performed to determine the efficiency of the immunoprecipitation.

Western blot

Protein extracts were prepared with NP40 lysis buffer supplemented with the protease inhibitor PMSF and cocktail. The prepared protein samples were subjected to polyacrylamide gel electrophoresis. The transferred polyvinylidene fluoride membrane was blocked with 5% skim milk at room temperature (RT) for 2 h. The primary antibody was incubated with

the transferred membrane at 4°C overnight, and the secondary antibodies were incubated at RT for 1 h. The primary antibodies included rabbit anti-ZSCAN4 (1:2,000, Sigma-Aldrich, AB4340), rabbit anti-ACTIN (1:10,000, ABclonal, AC026), rabbit anti-H3 (1:5,000, Abcam, ab1791-100 μg), rabbit anti-RIF1 (1:3,000, Abcam, ab13422), rat anti-TRF1 (1:2,000, Abcam, ab192629), rabbit anti-KAP1 (1:3,000, GeneTex, GTX102226), mouse anti-SUV39H1 (1:3,000, Abcam, ab12405), anti-HP1 (1:2000, Millipore, 05–689), anti-SETDB1 (1:2,000, Abcam, ab12317), G9A (1:2,000, CST, 3306S), GLP (1:1,000, R&D, PP-B0422-00), rabbit anti-H3K9me3 (1:2,000, Abcam, ab8898), rabbit anti-H3K27me3 (1:2,000, Millipore, 07-449), H3K9ac (1:2,000, Abcam, ab32129, 100 μL), goat anti-mouse IgG, horseradish peroxidase (HRP)-conjugated (Horseradish Peroxidase) (1:10,000, Abways Technology W, AB0102) or goat anti-rabbit HRP(1:10,000, Abways Technology W, AB0101). The SGO2A polyclonal antibody was produced by GenScript and targeted the short peptide KRQCVPLNLTEPSLRSKMRR (Gomez et al., 2007), and the antibody used was diluted 1:2,000.

Immunofluorescence microscopy

The samples were fixed at 4°C for 20 min in 4% paraformaldehyde (PFA), washed three times with PBS, permeabilized for 25 min, and sealed at RT for 2 h. The primary antibody was incubated overnight at 4°C, and the secondary antibody was incubated at RT for 1 h. The antibodies used were as follows: rabbit anti-SGO2A (1:200) and rat anti-TRF1 (1:200). The nuclei were stained with DAPI (1:200). The images were acquired by a CCD camera equipped with a laser scanning confocal microscope (Leica, TCS SP8).

Determination of the relative fluorescence intensity

To measure the fluorescence intensity via ImageJ, the measurement parameters were first set. The specific steps are as follows: Analyze-set measurements. Then, the area, mean, integrated density, etc. are selected. After that, the fluorescence image is opened, the fluorescent group is selected, and the menu bar Plugins-Analyze. By removing the background fluorescence signal in gray value using the same threshold values among all images, we can estimate the relative fluorescence intensity of each nucleus.

TRF measurement

TRF analysis was performed via a commercial kit (Telo TAGGG Telomere Length Assay, cat no. 12209136001, Roche). The cells were pretreated with RNase A and proteinase K (PCR Grade, 03115879001; Roche Life Science), followed by extraction with phenol:chloroform:isoamyl alcohol. A total of 3 μg of DNA was digested overnight with MboI endonuclease (NEB) at 37°C and subjected to electrophoresis via a CHEF Mapper pulsed-field electrophoresis system (Bio-Rad). Telomere length was quantified by TeloTool software.

Telomere Q-FISH

Telomere length was estimated via telomere Q-FISH as described previously (Poon et al., 1999). The cells were incubated with 0.3 μg/mL nocodazole for 3 h to enrich metaphases. Metaphase-enriched cells were subjected to hypotonic treatment with a 75 mM KCl solution, fixed with methanol:glacial acetic acid (3:1), and spread onto clean slides. Telomeres were denatured at 80°C and hybridized with a Cy3-labeled (CCCTAA)3 peptide nucleic acid (PNA) telomere probe (0.5 μg/mL) (Panagene, Korea). Chromosomes were stained with 0.5 μg/mL DAPI. Fluorescence from chromosomes and telomeres was digitally imaged on a Zeiss Axio Imager Z2 with Cy3/DAPI filters via AxioCam and AxioVision software. Telomere length, shown as telomere fluorescence intensity, was integrated via the TFL-TELO program (a gift kindly provided by Peter Lansdorp).

RNA-seq library construction

The RNA was disrupted at high temperature via the addition of divalent cations. First-strand cDNA was synthesized using the segmented mRNA as a template. Second-strand cDNA was then synthesized by adding dNTPs, DNA polymerase I, and RNase. Then, the DNA ends were converted to flat ends, and the 3′ end was adenylated. The NEBNext Adaptors connector was connected and ready for hybridization. The AMPure XP system (Beckman Coulter, Beverly, USA) was used to purify the library fragments. The target fragment was then ligated with 3 μL of USER enzyme (NEB, USA) at 37°C for 15 min, followed by 5 min at 95°C, after which PCR was performed. The PCR products were purified via the AMPure XP system. After quality assessment, the library was sequenced on an Illumina HiSeq platform.

CUT&Tag library construction

CUT&Tag was performed as previously described (Kaya-Okur et al., 2019), with minor modifications. Briefly, 100,000 cells per sample replicate were washed in wash buffer and then immobilized on 10 μL of concanavalin A-coated beads (Bangs Laboratories, BP531). The cells were incubated with the primary antibody H3K9me3 (1:100, Abcam, ab8898) at RT for 2 h on a shaker. The sections were incubated with a goat anti-rabbit IgG secondary antibody (1:100, Vazyme, Ab206-01-AC) at RT for 1 h. The cells were cleared on a magnetic rack and incubated with the addition of pA-Tn5 at RT for 1 h. The cells were subsequently washed with 700 μL of Dig-300 buffer, resuspended in 300 μL of tagmentation buffer, and incubated at 37°C for 1 h. A total of 10 μL of 0.5 M EDTA, 3 μL of 10% SDS, 2.5 μL of 20 mg/mL proteinase K, and 2 μL of spike-in DNA were added to the tube after being fully mixed and incubated at

37°C overnight. DNA was purified via phenol/chloroform/isoamyl alcohol extraction. The samples were subsequently amplified via PCR via the TruePrep Index Kit V4 for Illumina (Vazyme, TD204) and cleaned with VAHTS DNA Clean Beads (Vazyme, N411-01). Library quality was assessed on an Agilent Bioanalyzer 2100 system, and the library preparations were sequenced on an Illumina HiSeq platform.

Data analysis

CUT&Tag reads were aligned to the mouse mm10 genome via Bowtie2 (Langdon, 2015) with the default options. Bam files were obtained via SAMtools (v.1.9). Scatterplots, correlation plots, and heatmaps are displayed via deepTools (Ramirez et al., 2014). Figures illustrating these continuous tag counts over selected genomic intervals were created in the IGV browser (Thorvaldsdottir et al., 2013).

RNA-seq raw reads were first aligned to the mouse reference genome (mm10) via STAR software (Liao et al., 2014) with the default parameters. Expression matrix was generated by Featurecounts software (Dobin and Gingeras, 2015). DEGs (Differentially Expressed Genes) were calculated via the R package dEseq2 (Love et al., 2014), and the expression levels were represented by the FPKM. DEGs) were defined on the basis of the fold change in expression levels and false discovery rate (FDR) values. If the absolute fold change was >2 and the FDR value was <0.05, genes were considered to be differentially expressed. To compare the functions of the DEGs, we used the Metascape website (https://metascape.org/gp/index.html#/main/step1).

Functional annotation

Gene Ontology (GO) enrichment analysis of differentially expressed genes was implemented via the clusterProfiler R package (Yu et al., 2012) and DAVID (https://david.ncifcrf.gov/), in which gene length bias was corrected. GO terms with corrected p values less than 0.05 were considered significantly enriched in the DEGs. Bar plots were drawn via ggpubr and ggplot.

Quantification and statistical analysis

For qPCR, statistical tests were performed on the data from three biological replicates via a two-tailed unpaired t test. For statistical analyses of significance, a two-tailed unpaired t test was used. *$p < 0.05$, **$p < 0.01$, ***$p < 0.001$, and ****$p < 0.0001$ were considered statistically significant. The error bars represent the standard deviation of the mean of three independent experiments.

RESOURCE AVAILABILITY

Lead contact

Further information and requests for resources and reagents should be directed to and will be fulfilled by the lead contact, Lin Liu (liulin@nankai.edu.cn).

Materials availability

Any materials or cell lines described in this study will be made available upon request.

Data and code availability

The accession number for the Sgo2a knockout RNA-seq data reported in this paper is GSE252361, and the CUT&Tag dataset is CRA031625. Western blot source data have been deposited at Mendeley at https://doi.org/10.17632/cn88s8mf63.1. Any other data can be made available upon request.

ACKNOWLEDGMENTS

This study was supported by funding from the National Key Research and Development Program of China (2018YFA0107000), the National Natural Science Foundation of China (32030033, 82230052, and 32261160571), and the Haihe Laboratory of Cell Ecosystem Innovation Fund (22HHXBSS00029). We acknowledge Tianjin Novogene Technology for their high-throughput sequencing services. We thank Linlin Liu, JiaoYang, Haifeng Fu, and Jie Li for assisting with the experiments.

AUTHOR CONTRIBUTIONS

P.S. performed most of the experiments, analyzed the data, and prepared and wrote the manuscript; K.J. participated in telomere measurement, flow cytometry, and microscopic imaging. G.Y. performed the bioinformatics analyses; L.L. planned the project, designed the experiments, supervised the data analysis, and revised the manuscript.

DECLARATION OF INTERESTS

The authors declare that they have no competing interests.

SUPPLEMENTAL INFORMATION

Supplemental information can be found online at https://doi.org/10.1016/j.stemcr.2026.102824.

Received: February 26, 2025
Revised: January 27, 2026
Accepted: January 28, 2026

REFERENCES

Abe, K.I., Funaya, S., Tsukioka, D., Kawamura, M., Suzuki, Y., Suzuki, M.G., Schultz, R.M., and Aoki, F. (2018). Minor zygotic gene activation is essential for mouse preimplantation development. Proc. Natl. Acad. Sci. USA *115*, E6780–E6788. https://doi.org/10.1073/pnas.1804309115.

Akiyama, T., Xin, L., Oda, M., Sharov, A.A., Amano, M., Piao, Y., Cadet, J.S., Dudekula, D.B., Qian, Y., Wang, W., et al. (2015). Transient bursts of Zscan4 expression are accompanied by the rapid derepression of heterochromatin in mouse embryonic stem cells. DNA Res. *22*, 307–318. https://doi.org/10.1093/dnares/dsv013.

Aranega, A.E., and Franco, D. (2024). Posttranscriptional Regulation by Proteins and Noncoding RNAs. Adv. Exp. Med. Biol. *1441*, 313–339. https://doi.org/10.1007/978-3-031-44087-8_17.

Baker, C.L., and Pera, M.F. (2018). Capturing Totipotent Stem Cells. Cell Stem Cell *22*, 25–34. https://doi.org/10.1016/j.stem.2017.12.011.

Barral, A., Pozo, G., Ducrot, L., Papadopoulos, G.L., Sauzet, S., Oldfield, A.J., Cavalli, G., and Déjardin, J. (2022). SETDB1/NSD-dependent H3K9me3/H3K36me3 dual heterochromatin maintains gene expression profiles by bookmarking poised enhancers. Mol. Cell *82*, 816–832.e12. https://doi.org/10.1016/j.molcel.2021.12.037.

Callicott, R.J., and Womack, J.E. (2006). Real-time PCR assay for measurement of mouse telomeres. Comp. Med. *56*, 17–22.

Ciechanover, A., Gonen, H., Elias, S., and Mayer, A. (1990). Degradation of proteins by the ubiquitin-mediated proteolytic pathway. N. Biol. *2*, 227–234.

Cui, S., Jin, Z., Yu, T., Guo, C., He, Y., Kan, Y., Yan, L., and Wu, L. (2025). Effect of Glycosylation on the Enzymatic Degradation of D-Amino Acid-Containing Peptides. Molecules *30*, 441. https://doi.org/10.3390/molecules30030441.

Dan, J., Liu, Y., Liu, N., Chiourea, M., Okuka, M., Wu, T., Ye, X., Mou, C., Wang, L., Wang, L., et al. (2014). Rif1 maintains telomere length homeostasis of ESCs by mediating heterochromatin silencing. Dev. Cell *29*, 7–19. https://doi.org/10.1016/j.devcel.2014.03.004.

De Iaco, A., Coudray, A., Duc, J., and Trono, D. (2019). DPPA2 and DPPA4 are necessary to establish a 2C-like state in mouse embryonic stem cells. EMBO Rep. *20*, e47382. https://doi.org/10.15252/embr.201847382.

De Iaco, A., Planet, E., Coluccio, A., Verp, S., Duc, J., and Trono, D. (2017). DUX-family transcription factors regulate zygotic genome activation in placental mammals. Nat. Genet. *49*, 941–945. https://doi.org/10.1038/ng.3858.

Dobin, A., and Gingeras, T.R. (2015). Mapping RNA-seq Reads with STAR. Curr. Protoc. Bioinform. *51*, 11.14.1–11.14.19. https://doi.org/10.1002/0471250953.bi1114s51.

Eckersley-Maslin, M., Alda-Catalinas, C., Blotenburg, M., Kreibich, E., Krueger, C., and Reik, W. (2019). Dppa2 and Dppa4 directly regulate the Dux-driven zygotic transcriptional program. Genes Dev. *33*, 194–208. https://doi.org/10.1101/gad.321174.118.

Eckersley-Maslin, M.A., Alda-Catalinas, C., and Reik, W. (2018). Dynamics of the epigenetic landscape during the maternal-to-zygotic transition. Nat. Rev. Mol. Cell Biol. *19*, 436–450. https://doi.org/10.1038/s41580-018-0008-z.

El Yakoubi, W., Buffin, E., Cladière, D., Gryaznova, Y., Berenguer, I., Touati, S.A., Gómez, R., Suja, J.A., van Deursen, J.M., and Wassmann, K. (2017). Mps1 kinase-dependent Sgo2 centromere localisation mediates cohesin protection in mouse oocyte meiosis I. Nat. Commun. *8*, 694. https://doi.org/10.1038/s41467-017-00774-3.

Enriquez-Gasca, R., Gould, P.A., Tunbak, H., Conde, L., Herrero, J., Chittka, A., Beck, C.R., Gifford, R., and Rowe, H.M. (2023). Co-option of endogenous retroviruses through genetic escape from TRIM28 repression. Cell Rep. *42*, 112625. https://doi.org/10.1016/j.celrep.2023.112625.

Falco, G., Lee, S.L., Stanghellini, I., Bassey, U.C., Hamatani, T., and Ko, M.S.H. (2007). Zscan4: a novel gene expressed exclusively in late 2-cell embryos and embryonic stem cells. Dev. Biol. *307*, 539–550. https://doi.org/10.1016/j.ydbio.2007.05.003.

Fueyo, R., Judd, J., Feschotte, C., and Wysocka, J. (2022). Roles of transposable elements in the regulation of mammalian transcription. Nat. Rev. Mol. Cell Biol. *23*, 481–497. https://doi.org/10.1038/s41580-022-00457-y.

Gaurav, N., O'Hara, R., Hyder, U., Qin, W., Her, C., Romero, H., Kumar, A., Marcaida, M.J., Singh, R.K., Hovius, R., et al. (2025). The HP1 box of KAP1 organizes HP1alpha for silencing of endogenous retroviral elements in embryonic stem cells. Nat. Commun. *16*, 5066. https://doi.org/10.1038/s41467-025-60279-2.

Gomez, R., Valdeolmillos, A., Parra, M.T., Viera, A., Carreiro, C., Roncal, F., Rufas, J.S., Barbero, J.L., and Suja, J.A. (2007). Mammalian SGO2 appears at the inner centromere domain and redistributes depending on tension across centromeres during meiosis II and mitosis. EMBO Rep. *8*, 173–180. https://doi.org/10.1038/sj.embor.7400877.

Grow, E.J., Weaver, B.D., Smith, C.M., Guo, J., Stein, P., Shadle, S.C., Hendrickson, P.G., Johnson, N.E., Butterfield, R.J., Menafra, R., et al. (2021). p53 convergently activates Dux/DUX4 in embryonic stem cells and in facioscapulohumeral muscular dystrophy cell models. Nat. Genet. *53*, 1207–1220. https://doi.org/10.1038/s41588-021-00893-0.

Hendrickson, P.G., Doráis, J.A., Grow, E.J., Whiddon, J.L., Lim, J.W., Wike, C.L., Weaver, B.D., Pflueger, C., Emery, B.R., Wilcox, A.L., et al. (2017). Conserved roles of mouse DUX and human DUX4 in activating cleavage-stage genes and MERVL/HERVL retrotransposons. Nat. Genet. *49*, 925–934. https://doi.org/10.1038/ng.3844.

Hormoz, S., Singer, Z.S., Linton, J.M., Antebi, Y.E., Shraiman, B.I., and Elowitz, M.B. (2016). Inferring Cell-State Transition Dynamics from Lineage Trees and Endpoint Single-Cell Measurements. Cell Syst. *3*, 419–433.e8. https://doi.org/10.1016/j.cels.2016.10.015.

Hu, Z., Tan, D.E.K., Chia, G., Tan, H., Leong, H.F., Chen, B.J., Lau, M.S., Tan, K.Y.S., Bi, X., Yang, D., et al. (2020). Maternal factor NELFA drives a 2C-like state in mouse embryonic stem cells. Nat. Cell Biol. *22*, 175–186. https://doi.org/10.1038/s41556-019-0453-8.

Jukam, D., Shariati, S.A.M., and Skotheim, J.M. (2017). Zygotic Genome Activation in Vertebrates. Dev. Cell *42*, 316–332. https://doi.org/10.1016/j.devcel.2017.07.026.

Kanoh, J. (2018). Unexpected roles of a shugoshin protein at subtelomeres. Genes Genet. Syst. *92*, 127–133. https://doi.org/10.1266/ggs.17-00016.

Kawashima, S.A., Tsukahara, T., Langegger, M., Hauf, S., Kitajima, T.S., and Watanabe, Y. (2007). Shugoshin enables tension-generating attachment of kinetochores by loading Aurora to centromeres. Genes Dev. *21*, 420–435. https://doi.org/10.1101/gad.1497307.

Kaya-Okur, H.S., Wu, S.J., Codomo, C.A., Pledger, E.S., Bryson, T.D., Henikoff, J.G., Ahmad, K., and Henikoff, S. (2019). CUT&Tag for efficient epigenomic profiling of small samples and single cells. Nat. Commun. *10*, 1930. https://doi.org/10.1038/s41467-019-09982-5.

Kerrebrock, A.W., Moore, D.P., Wu, J.S., and Orr-Weaver, T.L. (1995). Mei-S332, a Drosophila protein required for sister-chromatid cohesion, can localize to meiotic centromere regions. Cell *83*, 247–256. https://doi.org/10.1016/0092-8674(95)90166-3.

Kitajima, T.S., Kawashima, S.A., and Watanabe, Y. (2004). The conserved kinetochore protein shugoshin protects centromeric cohesion during meiosis. Nature *427*, 510–517. https://doi.org/10.1038/nature02312.

Langdon, W.B. (2015). Performance of genetic programming optimised Bowtie2 on genome comparison and analytic testing (GCAT) benchmarks. BioData Min. *8*, 1. https://doi.org/10.1186/s13040-014-0034-0.

Le, R., Huang, Y., Zhang, Y., Wang, H., Lin, J., Dong, Y., Li, Z., Guo, M., Kou, X., Zhao, Y., et al. (2021). Dcaf11 activates Zscan4-mediated alternative telomere lengthening in early embryos and embryonic stem cells. Cell Stem Cell *28*, 732–747.e9. https://doi.org/10.1016/j.stem.2020.11.018.

Li, H., Sun, J., Dong, Y., Huang, Y., Wu, L., Xi, C., Su, Z., Xiao, Y., Zhang, C., Liang, Y., et al. (2023). Remodeling of H3K9me3 during the pluripotent to totipotent-like state transition. Stem Cell Rep. *18*, 449–462. https://doi.org/10.1016/j.stemcr.2022.12.006.

Li, P., Wang, L., Bennett, B.D., Wang, J., Li, J., Qin, Y., Takaku, M., Wade, P.A., Wong, J., and Hu, G. (2017). Rif1 promotes a repressive chromatin state to safeguard against endogenous retrovirus activation. Nucleic Acids Res. *45*, 12723–12738. https://doi.org/10.1093/nar/gkx884.

Liao, Y., Smyth, G.K., and Shi, W. (2014). featureCounts: an efficient general purpose program for assigning sequence reads to genomic features. Bioinformatics *30*, 923–930. https://doi.org/10.1093/bioinformatics/btt656.

Llano, E., Gómez, R., Gutiérrez-Caballero, C., Herrán, Y., Sánchez-Martín, M., Vázquez-Quiñones, L., Hernández, T., de Alava, E., Cuadrado, A., Barbero, J.L., et al. (2008). Shugoshin-2 is essential for the completion of meiosis but not for mitotic cell division in mice. Genes Dev. *22*, 2400–2413. https://doi.org/10.1101/gad.475308.

Love, M.I., Huber, W., and Anders, S. (2014). Moderated estimation of fold change and dispersion for RNA-seq data with DESeq2. Genome Biol. *15*, 550. https://doi.org/10.1186/s13059-014-0550-8.

Lv, T., He, D., Zhang, X., Guo, X., Li, Z., Zhang, A., Fan, B., and Wang, Z. (2022). SGOL2 promotes prostate cancer progression by inhibiting RAB1A ubiquitination. Aging (Albany NY) *14*, 10050–10066. https://doi.org/10.18632/aging.204443.

Macfarlan, T.S., Gifford, W.D., Driscoll, S., Lettieri, K., Rowe, H.M., Bonanomi, D., Firth, A., Singer, O., Trono, D., and Pfaff, S.L. (2012). Embryonic stem cell potency fluctuates with endogenous retrovirus activity. Nature *487*, 57–63. https://doi.org/10.1038/nature11244.

Maksakova, I.A., Thompson, P.J., Goyal, P., Jones, S.J., Singh, P.B., Karimi, M.M., and Lorincz, M.C. (2013). Distinct roles of KAP1, HP1 and G9a/GLP in silencing of the two-cell-specific retrotransposon MERVL in mouse ES cells. Epigenetics Chromatin *6*, 15. https://doi.org/10.1186/1756-8935-6-15.

Marston, A.L., Tham, W.H., Shah, H., and Amon, A. (2004). A genome-wide screen identifies genes required for centromeric cohesion. Science *303*, 1367–1370. https://doi.org/10.1126/science.1094220.

Mihalas, B.P., Pieper, G.H., Aboelenain, M., Munro, L., Srsen, V., Currie, C.E., Kelly, D.A., Hartshorne, G.M., Telfer, E.E., McAinsh, A.D., et al. (2024). Age-dependent loss of cohesion protection in human oocytes. Curr. Biol. *34*, 117–131.e5. https://doi.org/10.1016/j.cub.2023.11.061.

Min, S.W., Cho, S.H., Zhou, Y., Schroeder, S., Haroutunian, V., Seeley, W.W., Huang, E.J., Shen, Y., Masliah, E., Mukherjee, C., et al. (2010). Acetylation of tau inhibits its degradation and contributes to tauopathy. Neuron *67*, 953–966. https://doi.org/10.1016/j.neuron.2010.08.044.

Palma, L.G., Alvarez-Villanueva, D., Maqueda, M., Barrero, M., Iglesias, A., Bertran, J., Alvarez, D., Garcia-Prieto, C.A., Ballare, C., Rodriguez-Cortez, V., et al. (2025). Chromatin activity of IkappaBalpha mediates the exit from naive pluripotency. eLife *14*, RP102784. https://doi.org/10.7554/eLife.102784.

Peaston, A.E., Evsikov, A.V., Graber, J.H., de Vries, W.N., Holbrook, A.E., Solter, D., and Knowles, B.B. (2004). Retrotransposons regulate host genes in mouse oocytes and preimplantation embryos. Dev. Cell *7*, 597–606. https://doi.org/10.1016/j.devcel.2004.09.004.

Percharde, M., Lin, C.J., Yin, Y., Guan, J., Peixoto, G.A., Bulut-Karslioglu, A., Biechele, S., Huang, B., Shen, X., and Ramalho-Santos, M. (2018). A LINE1-Nucleolin Partnership Regulates Early Development and ESC Identity. Cell *174*, 391–405.e19. https://doi.org/10.1016/j.cell.2018.05.043.

Pinzon-Arteaga, C.A., O'Hara, R., Mazzagatti, A., Ballard, E., Hu, Y., Pan, A., Schmitz, D.A., Wei, Y., Sakurai, M., Ly, P., et al. (2024). TASOR expression in naive embryonic stem cells safeguards their developmental potential. Cell Rep. *43*, 114887. https://doi.org/10.1016/j.celrep.2024.114887.

Poon, S.S., Martens, U.M., Ward, R.K., and Lansdorp, P.M. (1999). Telomere length measurements using digital fluorescence microscopy. Cytometry *36*, 267–278. https://doi.org/10.1002/(sici)1097-0320(19990801)36:4<267::aid-cyto1>3.0.co;2-o.

Rabitsch, K.P., Gregan, J., Schleiffer, A., Javerzat, J.P., Eisenhaber, F., and Nasmyth, K. (2004). Two fission yeast homologs of Drosophila Mei-S332 are required for chromosome segregation during meiosis I and II. Curr. Biol. *14*, 287–301. https://doi.org/10.1016/j.cub.2004.01.051.

Ramirez, F., Dundar, F., Diehl, S., Gruning, B.A., and Manke, T. (2014). deepTools: a flexible platform for exploring deep-sequencing data. Nucleic Acids Res. *42*, W187–W191. https://doi.org/10.1093/nar/gku365.

Rodriguez-Terrones, D., Gaume, X., Ishiuchi, T., Weiss, A., Kopp, A., Kruse, K., Penning, A., Vaquerizas, J.M., Brino, L., and Torres-Padilla, M.E. (2018). A molecular roadmap for the emergence of early-embryonic-like cells in culture. Nat. Genet. *50*, 106–119. https://doi.org/10.1038/s41588-017-0016-5.

Rowe, H.M., Kapopoulou, A., Corsinotti, A., Fasching, L., Macfarlan, T.S., Tarabay, Y., Viville, S., Jakobsson, J., Pfaff, S.L., and Trono, D. (2013). TRIM28 repression of retrotransposon-based enhancers

is necessary to preserve transcriptional dynamics in embryonic stem cells. Genome Res. *23*, 452–461. https://doi.org/10.1101/gr.147678.112.

Salic, A., Waters, J.C., and Mitchison, T.J. (2004). Vertebrate shugoshin links sister centromere cohesion and kinetochore microtubule stability in mitosis. Cell *118*, 567–578. https://doi.org/10.1016/j.cell.2004.08.016.

Shi, P., Lu, X., Jin, K., Liu, L., Yin, G., Wang, W., Yang, J., Wang, L., Dong, L., Xie, W., and Liu, L. (2025). USP17L promotes the 2-cell-like program through deubiquitination of H2AK119ub1 and ZSCAN4. Nat. Commun. *16*, 7071. https://doi.org/10.1038/s41467-025-62303-x.

Spencley, A.L., Bar, S., Swigut, T., Flynn, R.A., Lee, C.H., Chen, L.F., Bassik, M.C., and Wysocka, J. (2023). Co-transcriptional genome surveillance by HUSH is coupled to termination machinery. Mol. Cell *83*, 1623–1639.e8. https://doi.org/10.1016/j.molcel.2023.04.014.

Sun, Q., Liu, F., Mo, X., Yao, B., Liu, G., Chen, S., and Ren, Y. (2022). Shugoshin Regulates Cohesin, Kinetochore-Microtubule Attachments, and Chromosomal Instability. Cytogenet. Genome Res. *162*, 283–296. https://doi.org/10.1159/000528141.

Tashiro, S., Handa, T., Matsuda, A., Ban, T., Takigawa, T., Miyasato, K., Ishii, K., Kugou, K., Ohta, K., Hiraoka, Y., et al. (2016). Shugoshin forms a specialized chromatin domain at subtelomeres that regulates transcription and replication timing. Nat. Commun. *7*, 10393. https://doi.org/10.1038/ncomms10393.

Thorvaldsdottir, H., Robinson, J.T., and Mesirov, J.P. (2013). Integrative Genomics Viewer (IGV): high-performance genomics data visualization and exploration. Briefings Bioinf. *14*, 178–192. https://doi.org/10.1093/bib/bbs017.

Tsukahara, T., Tanno, Y., and Watanabe, Y. (2010). Phosphorylation of the CPC by Cdk1 promotes chromosome bi-orientation. Nature *467*, 719–723. https://doi.org/10.1038/nature09390.

van Steensel, B., and de Lange, T. (1997). Control of telomere length by the human telomeric protein TRF1. Nature *385*, 740–743. https://doi.org/10.1038/385740a0.

Vanoosthuyse, V., Prykhozhij, S., and Hardwick, K.G. (2007). Shugoshin 2 regulates localization of the chromosomal passenger proteins in fission yeast mitosis. Mol. Biol. Cell *18*, 1657–1669. https://doi.org/10.1091/mbc.e06-10-0890.

Vaur, S., Cubizolles, F., Plane, G., Genier, S., Rabitsch, P.K., Gregan, J., Nasmyth, K., Vanoosthuyse, V., Hardwick, K.G., and Javerzat, J.P. (2005). Control of Shugoshin function during fission-yeast meiosis. Curr. Biol. *15*, 2263–2270. https://doi.org/10.1016/j.cub.2005.11.034.

Walsh, C.P., Chaillet, J.R., and Bestor, T.H. (1998). Transcription of IAP endogenous retroviruses is constrained by cytosine methylation. Nat. Genet. *20*, 116–117. https://doi.org/10.1038/2413.

Wang, C., Songyang, Z., and Huang, Y. (2021). TRIM28 inhibits alternative lengthening of telomere phenotypes by protecting SETDB1 from degradation. Cell Biosci. *11*, 149. https://doi.org/10.1186/s13578-021-00660-y.

Wang, X., Li, Y., He, M., Kong, X., Jiang, P., Liu, X., Diao, L., Zhang, X., Li, H., Ling, X., et al. (2022). UbiBrowser 2.0: a comprehensive resource for proteome-wide known and predicted ubiquitin ligase/deubiquitinase-substrate interactions in eukaryotic species. Nucleic Acids Res. *50*, D719–D728. https://doi.org/10.1093/nar/gkab962.

Watanabe, Y. (2005). Shugoshin: guardian spirit at the centromere. Curr. Opin. Cell Biol. *17*, 590–595. https://doi.org/10.1016/j.ceb.2005.10.003.

Weber, B., Horiguchi, J., Luebbers, R., Sherman, M., and Kufe, D. (1989). Posttranscriptional stabilization of c-fms mRNA by a labile protein during human monocytic differentiation. Mol. Cell Biol. *9*, 769–775. https://doi.org/10.1128/mcb.9.2.769-775.1989.

Wen, Q., Zhou, J., Tian, C., Li, X., Song, G., Gao, Y., Sun, Y., Ma, C., Yao, S., Liang, X., et al. (2023). Symmetric inheritance of parental histones contributes to safeguarding the fate of mouse embryonic stem cells during differentiation. Nat. Genet. *55*, 1555–1566. https://doi.org/10.1038/s41588-023-01477-w.

Whiddon, J.L., Langford, A.T., Wong, C.J., Zhong, J.W., and Tapscott, S.J. (2017). Conservation and innovation in the DUX4-family gene network. Nat. Genet. *49*, 935–940. https://doi.org/10.1038/ng.3846.

Wu, J., Huang, B., Chen, H., Yin, Q., Liu, Y., Xiang, Y., Zhang, B., Liu, B., Wang, Q., Xia, W., et al. (2016). The landscape of accessible chromatin in mammalian preimplantation embryos. Nature *534*, 652–657. https://doi.org/10.1038/nature18606.

Wu, K., Liu, H., Wang, Y., He, J., Xu, S., Chen, Y., Kuang, J., Liu, J., Guo, L., Li, D., et al. (2020). SETDB1-Mediated Cell Fate Transition between 2C-Like and Pluripotent States. Cell Rep. *30*, 25–36.e6. https://doi.org/10.1016/j.celrep.2019.12.010.

Xiong, Z., Xu, K., Lin, Z., Kong, F., Wang, Q., Quan, Y., Sha, Q.Q., Li, F., Zou, Z., Liu, L., et al. (2022). Ultrasensitive Ribo-seq reveals translational landscapes during mammalian oocyte-to-embryo transition and pre-implantation development. Nat. Cell Biol. *24*, 968–980. https://doi.org/10.1038/s41556-022-00928-6.

Xu, Q., and Xie, W. (2018). Epigenome in Early Mammalian Development: Inheritance, Reprogramming and Establishment. Trends Cell Biol. *28*, 237–253. https://doi.org/10.1016/j.tcb.2017.10.008.

Xu, R., Li, C., Liu, X., and Gao, S. (2021). Insights into epigenetic patterns in mammalian early embryos. Protein Cell *12*, 7–28. https://doi.org/10.1007/s13238-020-00757-z.

Yamamoto, H., Uchida, Y., Kurimoto, R., Chiba, T., Matsushima, T., Ito, Y., Inotsume, M., Miyata, K., Watanabe, K., Inada, M., et al. (2023). RNA-binding protein LIN28A upregulates transcription factor HIF1alpha by posttranscriptional regulation via direct binding to UGAU motifs. J. Biol. Chem. *299*, 102791. https://doi.org/10.1016/j.jbc.2022.102791.

Yan, Y.L., Zhang, C., Hao, J., Wang, X.L., Ming, J., Mi, L., Na, J., Hu, X., and Wang, Y. (2019). DPPA2/4 and SUMO E3 ligase PIAS4 opposingly regulate zygotic transcriptional program. PLoS Biol. *17*, e3000324. https://doi.org/10.1371/journal.pbio.3000324.

Yang, J., Dan, J., Zhao, N., Liu, L., Wang, H., Liu, Q., Wang, L., Li, J., Wu, Y., Chen, F., et al. (2024). Zscan4 mediates ubiquitination and degradation of the corepressor complex to promote chromatin accessibility in 2C-like cells. Proc. Natl. Acad. Sci. USA *121*, e2407490121. https://doi.org/10.1073/pnas.2407490121.

Ye, X., Tian, C., Liu, L., Feng, G., Jin, K., Wang, H., Chen, J., and Liu, L. (2021). Oncostatin M Maintains Naive Pluripotency of mESCs

by Tetraploid Embryo Complementation (TEC) Assay. Front. Cell Dev. Biol. *9*, 675411. https://doi.org/10.3389/fcell.2021.675411.

Yoshizawa-Sugata, N., Yamazaki, S., Mita-Yoshida, K., Ono, T., Nishito, Y., and Masai, H. (2021). Loss of full-length DNA replication regulator Rif1 in two-cell embryos is associated with zygotic transcriptional activation. J. Biol. Chem. *297*, 101367. https://doi.org/10.1016/j.jbc.2021.101367.

Yu, G., Wang, L.G., Han, Y., and He, Q.Y. (2012). clusterProfiler: an R package for comparing biological themes among gene clusters. OMICS *16*, 284–287. https://doi.org/10.1089/omi.2011.0118.

Yu, H., Sun, Z., Tan, T., Pan, H., Zhao, J., Zhang, L., Chen, J., Lei, A., Zhu, Y., Chen, L., et al. (2021). rRNA biogenesis regulates mouse 2C-like state by 3D structure reorganization of peri-nucleolar heterochromatin. Nat. Commun. *12*, 6365. https://doi.org/10.1038/s41467-021-26576-2.

Zalzman, M., Falco, G., Sharova, L.V., Nishiyama, A., Thomas, M., Lee, S.L., Stagg, C.A., Hoang, H.G., Yang, H.T., Indig, F.E., et al. (2010). Zscan4 regulates telomere elongation and genomic stability in ES cells. Nature *464*, 858–863. https://doi.org/10.1038/nature08882.

Zhang, B., Zheng, H., Huang, B., Li, W., Xiang, Y., Peng, X., Ming, J., Wu, X., Zhang, Y., Xu, Q., et al. (2016). Allelic reprogramming of the histone modification H3K4me3 in early mammalian development. Nature *537*, 553–557. https://doi.org/10.1038/nature19361.

Zhang, J., Donahue, G., Gilbert, M.B., Lapidot, T., Nicetto, D., and Zaret, K.S. (2024). Distinct H3K9me3 heterochromatin maintenance dynamics govern different gene programmes and repeats in pluripotent cells. Nat. Cell Biol. *26*, 2115–2128. https://doi.org/10.1038/s41556-024-01547-z.

Zhang, K., Wu, D.Y., Zheng, H., Wang, Y., Sun, Q.R., Liu, X., Wang, L.Y., Xiong, W.J., Wang, Q., Rhodes, J.D.P., et al. (2020). Analysis of Genome Architecture during SCNT Reveals a Role of Cohesin in Impeding Minor ZGA. Mol. Cell *79*, 234–250.e9. https://doi.org/10.1016/j.molcel.2020.06.001.

Zhang, W., Chen, F., Chen, R., Xie, D., Yang, J., Zhao, X., Guo, R., Zhang, Y., Shen, Y., Göke, J., et al. (2019). Zscan4c activates endogenous retrovirus MERVL and cleavage embryo genes. Nucleic Acids Res. *47*, 8485–8501. https://doi.org/10.1093/nar/gkz594.

Zhou, S., Guo, Y., Sun, H., Liu, L., Yao, L., Liu, C., He, Y., Cao, S., Zhou, C., Li, M., et al. (2021). Maternal RNF114-mediated target substrate degradation regulates zygotic genome activation in mouse embryos. Development *148*, dev199426. https://doi.org/10.1242/dev.199426.

Stem Cell Reports, Volume *21*

Supplemental Information

Shugoshin 2A stabilizes heterochromatin complexes to suppress the 2-cell-like state in embryonic stem cells

Panpan Shi, Kairang Jin, Guoxing Yin, and Lin Liu

Supplemental Information

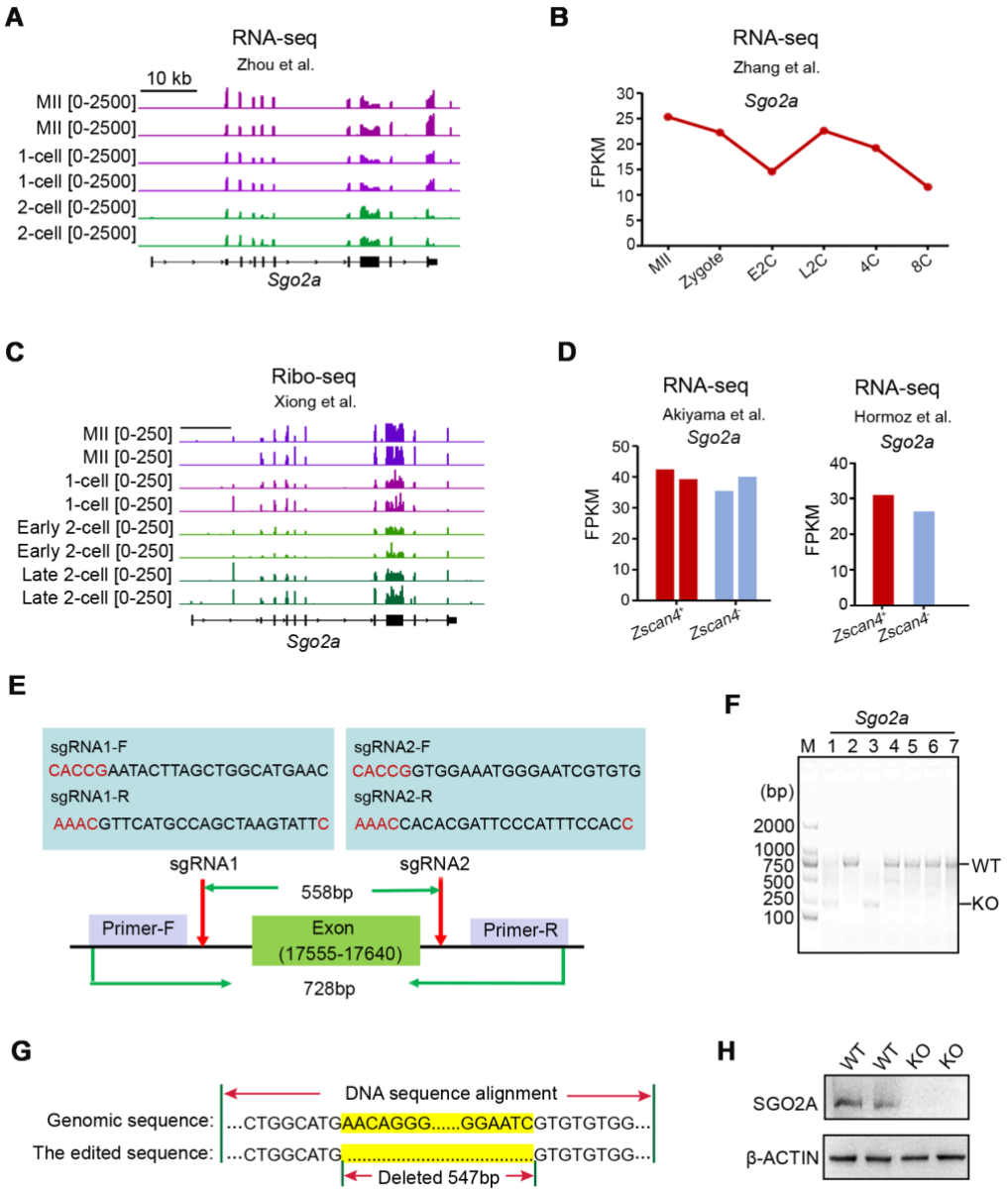

Supplemental Figure S1. Dynamic expression of *Sgo2a* in early mouse embryos and ESCs, and the *Sgo2a* knockout strategy. (A) IGV plot displaying the expression level of *Sgo2a* in early mouse embryos(Zhou et al., 2021). **(B)** RNA-Seq data showing the expression level of *Sgo2a* in early mouse embryos(Zhang et al., 2016). **(C)** Ribo-seq image showing the translational landscape of *Sgo2a* in early embryos(Xiong et al., 2022). **(D)** Expression levels of *Sgo2a* in *Zscan4*$^{+}$ and *Zscan4*$^{-}$ ESCs determined via RNA-Seq(Akiyama et al., 2015; Hormoz et al., 2016). **(E)** *Sgo2a* gene editing

sites and sgRNA display. An exon (17555--17640) is knocked out. **(F)** Nucleic acid gel electrophoresis showing the genetic test results of *Sgo2a* knockout. **(G)** DNA sequencing results showing that the exon (17555--17640) of *Sgo2a* was knocked out. **(H)** SGO2A knockout was detected via Western blot.

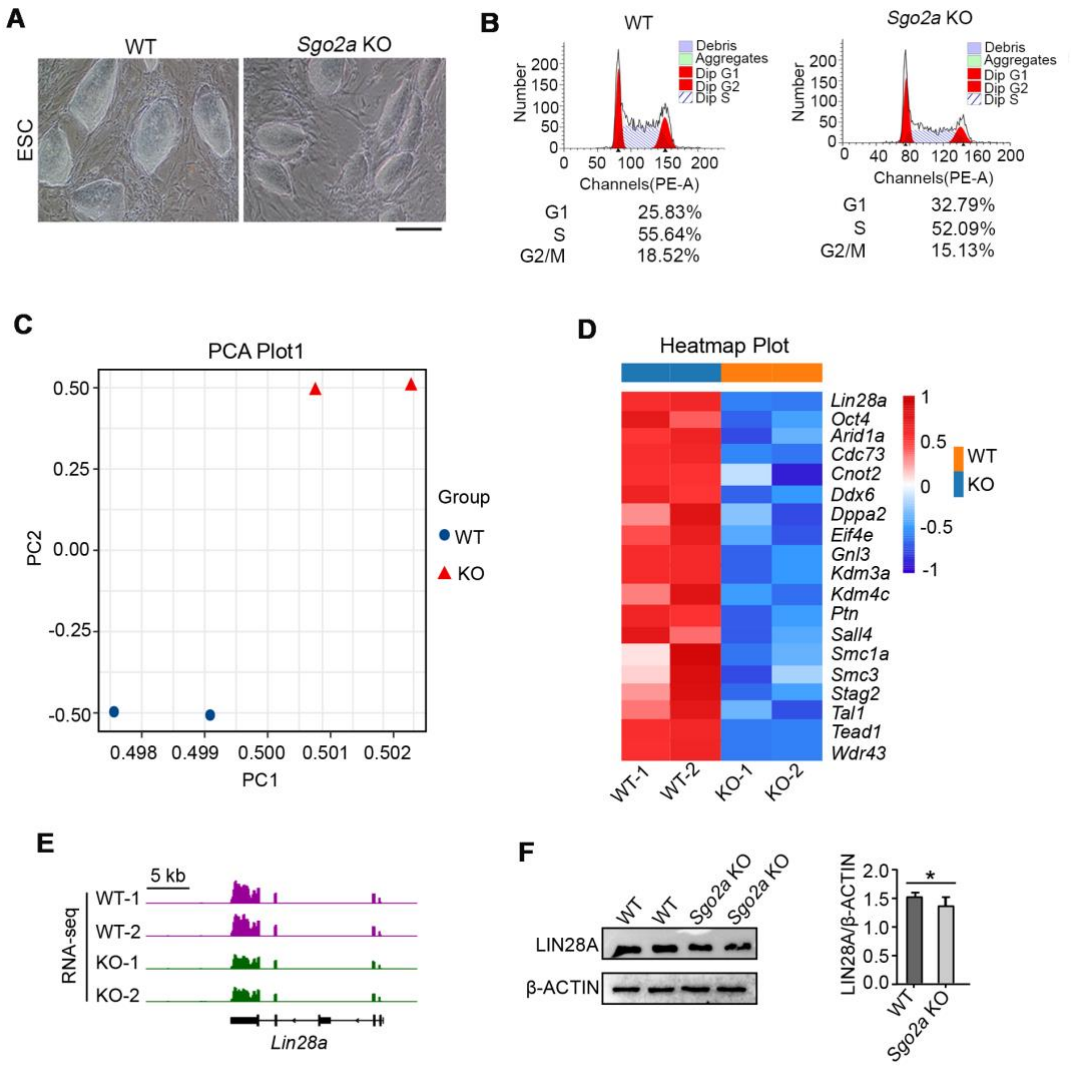

Supplemental Figure S2. *Sgo2a* deficiency affects the cell cycle and pluripotency. (A) Clonal display of WT and *Sgo2a*-deficient ESCs. Scale bar, 100μm. **(B)** Cell cycle measurement of WT and *Sgo2a*-deficient ESCs. **(C)** RNA-Seq data were used to analyze the consistency between repeated samples. **(D)** Heatmap showing the downregulation of pluripotent genes. The colors from blue to red in ascending order represent gene expression from low to high. **(E)** IGV plot displaying the expression level of *Lin28a* in WT and *Sgo2a* knockout ESCs. **(F)** Western blot showing changes in LIN28A protein levels after *Sgo2a* knockout. The right graph shows LIN28A compared with β-ACTIN (n=3 independent experiments). Data were shown as means ± SD (two-tailed Student's t-test). *P < 0.05.

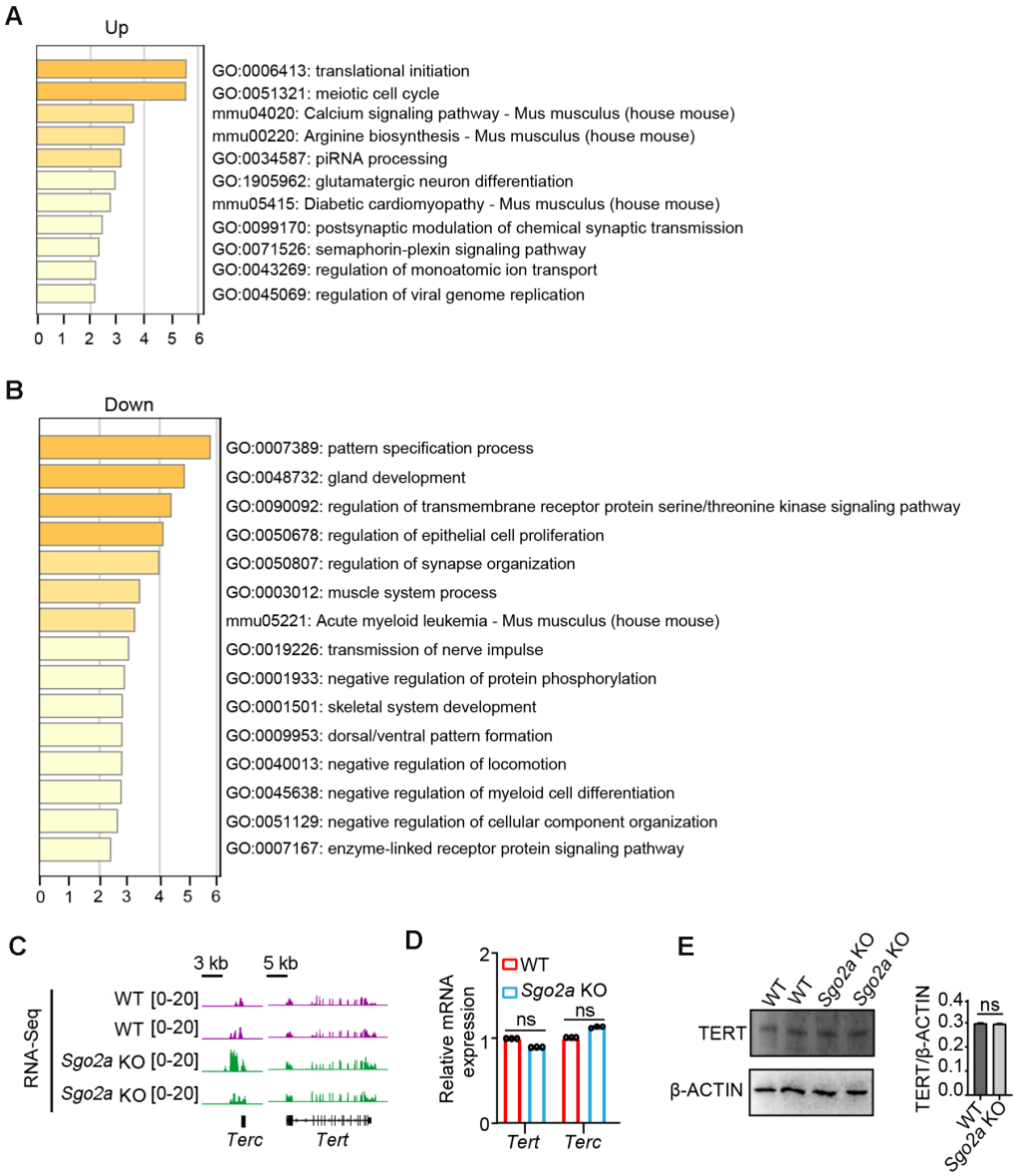

Supplemental Figure S3. *Sgo2a* knockout influences other biological processes. (A-B) RNA-Seq analysis of life processes affected by *Sgo2a* knockout. **(C)** IGV plot displaying the expression levels of *Terc and Tert* in WT and *Sgo2a* knockout ESCs. **(D)** qPCR results showing the expression levels of *Terc and Tert* in WT and *Sgo2a* knockout ESCs (n=3 independent experiments). Data were shown as means ± SD (two-tailed Student's t-test). **(E)** Western Blot results showing the expression levels of TERT in WT and *Sgo2a* knockout ESCs. The right graph shows TERT compared with β-ACTIN (n=3 independent experiments). Data were shown as means ± SD (two-tailed Student's t-test).

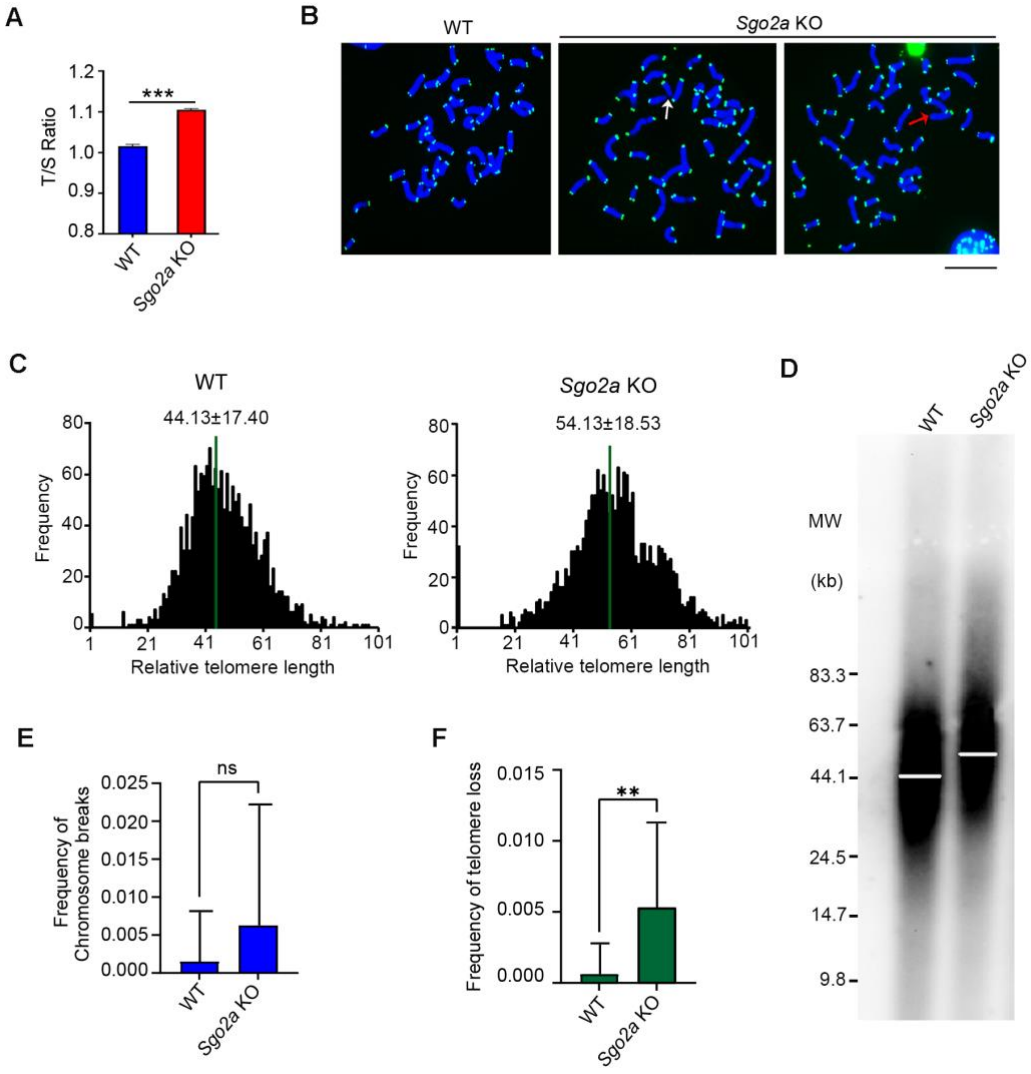

Supplemental Figure S4. *Sgo2a* deficiency lengthens telomeres. (A) qPCR was used to detect changes in telomere length following the knockout of *Sgo2a* (n=3 independent experiments). Data were shown as means ± SD (two-tailed Student's t-test); ***P < 0.001. **(B)** Micrographs showing telomeres by Q-FISH. White arrow, chromosome breakage. Red arrow, telomere loss. Scale bar, 100μm. **(C)** Telomere length analysis via TFL-TELO software. The green lines indicate the median telomere length. The average length ± SD is given above. *P < 0.05; ***P < 0.001. **(D)** TRF by Southern blot demonstrating telomere length variation. **(E)** The frequency of chromosome breakage (n=20 spreads). **(F)** The frequency of telomere loss (n=20 spreads).

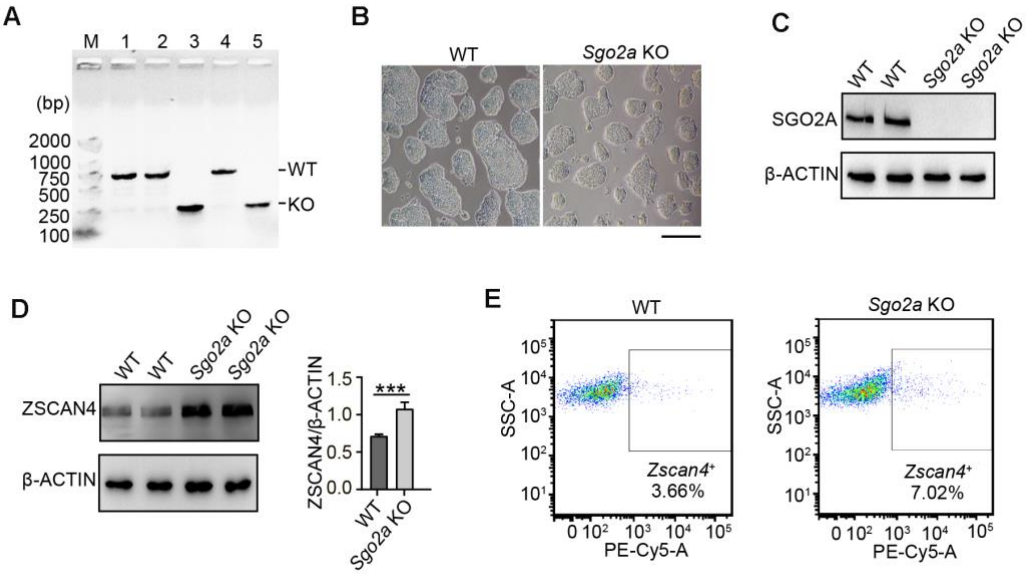

Supplemental Figure S5. *Sgo2a* deficiency increases the proportion of *Zscan4*⁺ cells. (A) Nucleic acid gel electrophoresis showing the genetic test results of *Sgo2a* knockout. **(B)** Clonal display of WT and *Sgo2a*-deficient ESCs. Scale bar, 100μm. **(C)** *Sgo2a* knockout was detected via Western blot. **(D)** Western blot showing the changes in ZSCAN4 after *Sgo2a* knockout. Right graph showing the quantification of ZSCAN4 compared with β-ACTIN (n=3 independent experiments). Data were shown as means ± SD (two-tailed Student's t-test); ***P < 0.001. **(E)** Flow cytometry analysis of the proportion of *Zscan4*⁺ cells.

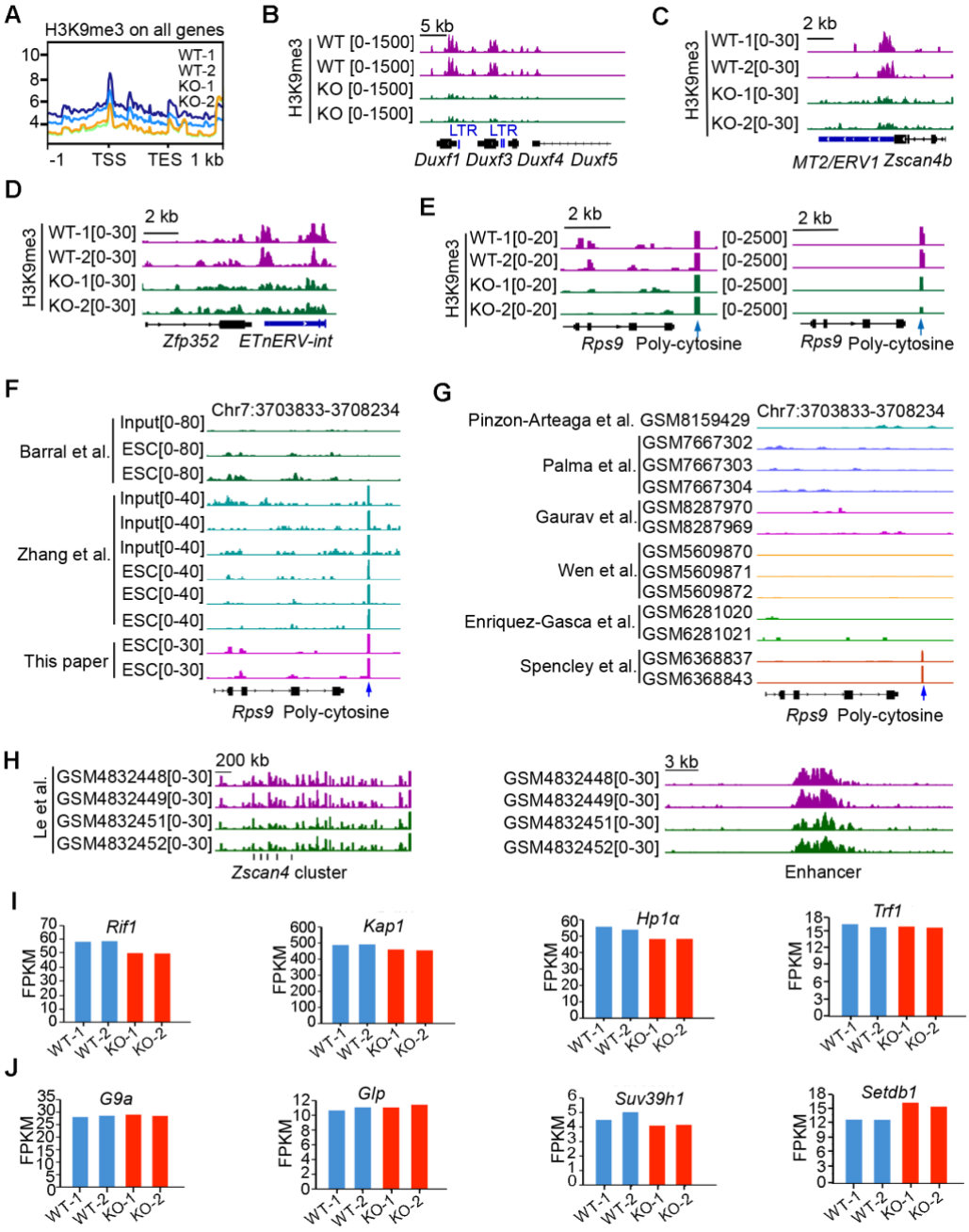

Supplemental Figure S6. SGO2A regulates H3K9me3 but does not affect the transcription of the H3K9 methylation complex and modifiers. (A) IGV shows the enrichment of H3K9me3 throughout the entire genome. **(B)** IGV shows the LTR within the TES-2kb region of *Dux* family. **(C-D)** IGV shows the transposable elements within the TES-2kb region of *Zscan4* **(C)** and *Zfp352* **(D)**, as well as the strong signal of H3K9me3. **(E)** IGV reveals the peak signal of H3K9me3 near *Rps9*. **(F)** Comparative analysis of the H3K9me3 signal near *Rps9*. The public data are derived from published literature(Barral et al., 2022; Zhang et al., 2024). **(G)** Analysis of the H3K9me3 signal near *Rps9*. The public

data are derived from published literature(Enriquez-Gasca et al., 2023; Gaurav et al., 2025; Palma et al., 2025; Pinzon-Arteaga et al., 2024; Spencley et al., 2023; Wen et al., 2023). **(H)** IGV plot displaying the enrichment of H3K9me3 on the *Zscan4* gene cluster and downstream enhancer(Le et al., 2021). Purple represents WT ESC; Green represents *Dcaf11* OE ESC. **(I-J)** Detection of H3K9me3 methylation-related genes by RNA-Seq in WT and *Sgo2a*-deficient ESCs.

Suppemental Table S1. Primers for RT–PCR.

Usp17l-F	TCCTTCCCAGAAGAGACTGGA
Usp17l-R	AGCAACCACCATGTCTCCAA
Zscan4-F	AAATGCCTTATGTCTGTTCCCTATG
Zscan4-R	TGTGGTAATTCCTCAGGTGACGAT
Tcstv1-F	TGAACCCTGATGCCTGCTAAGACT
Tcstv1-R	AGATGGCTGCAAAGACACAACTGC
MERVL-F	AAGGGGTGGATTGTAGTGGC
MERVL-R	GTCACTGGTGAGCCTTCCAA

Supplemental Methods

Generation of knockout (KO) ESCs via SgRNA

sgRNAs were designed for the *Sgo2a* knockout experiment via the online design sgRNA (https://www.zlab.bio/guide-design-resources). The sequence of the sgRNAs was as follows:

Sgo2a-sgRNA-F: CACCGAATACTTAGCTGGCATGAAC

Sgo2a-sgRNA-R: AAACGTTCATGCCAGCTAAGTATTC

Single-stranded SgRNA was annealed into double-stranded sgRNA, and a knockdown vector was subsequently constructed. The annealing procedure was 95°C for 30 s, 72°C for 2 min, 56°C for 2 min, 37°C for 2 min, 25°C for 2 min, and storage at 4°C. The resulting double-stranded DNA is subsequently inserted into the knockout vector. The plasmids were transfected into ESCs via the Lonza nuclear transfer apparatus. After 24 h, 1.5 μg/ml puromycin was added for screening, and the *Sgo2a* knockout cell clone was subsequently selected for culture identification. Stable *Sgo2a* knockout ESCs were then selected with 1.5 μg/ml puromycin for one week.

Telomere restriction fragment (TRF) measurement

TRF analysis was performed via a commercial kit (Telo TAGGG Telomere Length Assay, cat no. 12209136001, Roche). The cells were pretreated with

RNase A and proteinase K (PCR Grade, 03115879001; Roche Life Science), followed by extraction with phenol:chloroform:isoamyl alcohol. A total of 3 μg of DNA was digested overnight with MboI endonuclease (NEB) at 37 °C and subjected to electrophoresis via a CHEF Mapper pulsed-field electrophoresis system (Bio-Rad). Telomere length was quantified by Telo Tool software.

Telomere quantitative fluorescence in situ hybridization (Q-FISH)

Telomere length was estimated via telomere Q-FISH as described previously(Poon et al., 1999). The cells were incubated with 0.3 μg/ml nocodazole for 3 h to enrich metaphases. Metaphase-enriched cells were subjected to hypotonic treatment with a 75 mM KCl solution, fixed with methanol:glacial acetic acid (3:1), and spread onto clean slides. Telomeres were denatured at 80 °C and hybridized with a Cy3-labeled (CCCTAA)3 peptide nucleic acid (PNA) telomere probe (0.5 μg/ml) (Panagene, Korea). Chromosomes were stained with 0.5 μg/ml DAPI. Fluorescence from chromosomes and telomeres was digitally imaged on a Zeiss Axio Imager Z2 with Cy3/DAPI filters via AxioCam and AxioVision software. Telomere length, shown as telomere fluorescence intensity, was integrated via the TFL-TELO program (a gift kindly provided by Peter Lansdorp).

Western blot

Protein extracts were prepared with NP40 lysis buffer supplemented with the protease inhibitor PMSF and cocktail. The prepared protein samples were subjected to polyacrylamide gel electrophoresis. The transferred PVDF membrane was blocked with 5% skim milk at room temperature for 2 h. The primary antibody was incubated with the transferred membrane at 4°C overnight, and the secondary antibodies were incubated at room temperature for 1 h. The primary antibodies included rabbit anti-Zscan4 (1:2000, Sigma–Aldrich, AB4340), rabbit anti-Actin (1:10000, ABclonal, AC026), goat anti-mouse HRP (1:10000, ABWAYS TECHNOLOGY W, AB0102) or goat anti-rabbit HRP (1:10000, ABWAYS TECHNOLOGY W, AB0101). The Sgo2a polyclonal antibody was produced by GenScript and targeted the short peptide KRQCVPLNLTEPSLRSKMRR(Gomez et al., 2007), and the antibody used was diluted 1:2000.

References

Akiyama, T., Xin, L., Oda, M., Sharov, A.A., Amano, M., Piao, Y., Cadet, J.S., Dudekula, D.B., Qian, Y., Wang, W., et al. (2015). Transient bursts of Zscan4 expression are accompanied by the rapid derepression of heterochromatin in mouse embryonic stem cells. DNA Res *22*, 307-318. 10.1093/dnares/dsv013.

Barral, A., Pozo, G., Ducrot, L., Papadopoulos, G.L., Sauzet, S., Oldfield, A.J., Cavalli, G., and Dejardin, J. (2022). SETDB1/NSD-dependent H3K9me3/H3K36me3 dual heterochromatin maintains gene expression profiles by bookmarking poised enhancers. Mol Cell *82*, 816-832 e812. 10.1016/j.molcel.2021.12.037.

Enriquez-Gasca, R., Gould, P.A., Tunbak, H., Conde, L., Herrero, J., Chittka, A., Beck, C.R., Gifford, R., and Rowe, H.M. (2023). Co-option of endogenous retroviruses through genetic escape from TRIM28 repression. Cell Rep *42*, 112625. 10.1016/j.celrep.2023.112625.

Gaurav, N., O'Hara, R., Hyder, U., Qin, W., Her, C., Romero, H., Kumar, A., Marcaida, M.J., Singh, R.K., Hovius, R., et al. (2025). The HP1 box of KAP1 organizes HP1alpha for silencing of endogenous retroviral elements in embryonic stem cells. Nat Commun *16*, 5066. 10.1038/s41467-025-60279-2.

Gomez, R., Valdeolmillos, A., Parra, M.T., Viera, A., Carreiro, C., Roncal, F., Rufas, J.S., Barbero, J.L., and Suja, J.A. (2007). Mammalian SGO2 appears at the inner centromere domain and redistributes depending on tension across centromeres during meiosis II and mitosis. EMBO Rep *8*, 173-180. 10.1038/sj.embor.7400877.

Hormoz, S., Singer, Z.S., Linton, J.M., Antebi, Y.E., Shraiman, B.I., and Elowitz, M.B. (2016). Inferring Cell-State Transition Dynamics from Lineage Trees and Endpoint Single-Cell Measurements. Cell Syst *3*, 419-433 e418. 10.1016/j.cels.2016.10.015.

Le, R., Huang, Y., Zhang, Y., Wang, H., Lin, J., Dong, Y., Li, Z., Guo, M., Kou, X., Zhao, Y., et al. (2021). Dcaf11 activates Zscan4-mediated alternative telomere lengthening in early embryos and embryonic stem cells. Cell Stem Cell *28*, 732-747 e739. 10.1016/j.stem.2020.11.018.

Palma, L.G., Alvarez-Villanueva, D., Maqueda, M., Barrero, M., Iglesias, A., Bertran, J., Alvarez, D., Garcia-Prieto, C.A., Ballare, C., Rodriguez-Cortez, V., et al. (2025). Chromatin activity of IkappaBalpha mediates the exit from naive pluripotency. Elife *14*. 10.7554/eLife.102784.

Pinzon-Arteaga, C.A., O'Hara, R., Mazzagatti, A., Ballard, E., Hu, Y., Pan, A., Schmitz, D.A., Wei, Y., Sakurai, M., Ly, P., et al. (2024). TASOR expression in naive embryonic stem cells safeguards their developmental potential. Cell Rep *43*, 114887. 10.1016/j.celrep.2024.114887.

Poon, S.S., Martens, U.M., Ward, R.K., and Lansdorp, P.M. (1999). Telomere length measurements using digital fluorescence microscopy. Cytometry *36*, 267-278. 10.1002/(sici)1097-0320(19990801)36:4<267::aid-cyto1>3.0.co;2-o.

Spencley, A.L., Bar, S., Swigut, T., Flynn, R.A., Lee, C.H., Chen, L.F., Bassik, M.C., and Wysocka, J. (2023). Co-transcriptional genome surveillance by HUSH is coupled to termination machinery. Mol Cell *83*, 1623-1639 e1628. 10.1016/j.molcel.2023.04.014.

Wen, Q., Zhou, J., Tian, C., Li, X., Song, G., Gao, Y., Sun, Y., Ma, C., Yao, S., Liang, X., et al. (2023). Symmetric inheritance of parental histones contributes to safeguarding the fate of mouse embryonic stem cells during differentiation. Nat Genet *55*, 1555-1566. 10.1038/s41588-023-01477-w.

Xiong, Z., Xu, K., Lin, Z., Kong, F., Wang, Q., Quan, Y., Sha, Q.Q., Li, F., Zou, Z., Liu, L., et al. (2022). Ultrasensitive Ribo-seq reveals translational landscapes during mammalian oocyte-to-embryo transition and pre-implantation development. Nat Cell Biol *24*, 968-980. 10.1038/s41556-022-00928-6.

Zhang, B., Zheng, H., Huang, B., Li, W., Xiang, Y., Peng, X., Ming, J., Wu, X., Zhang, Y., Xu, Q., et al. (2016). Allelic reprogramming of the histone modification H3K4me3 in early mammalian development. Nature *537*, 553-557. 10.1038/nature19361.

Zhang, J., Donahue, G., Gilbert, M.B., Lapidot, T., Nicetto, D., and Zaret, K.S. (2024). Distinct H3K9me3 heterochromatin maintenance dynamics govern different gene programmes and repeats in pluripotent cells. Nat Cell Biol *26*, 2115-2128. 10.1038/s41556-024-01547-z.

Zhou, S., Guo, Y., Sun, H., Liu, L., Yao, L., Liu, C., He, Y., Cao, S., Zhou, C., Li, M., et al. (2021). Maternal RNF114-mediated target substrate degradation regulates zygotic genome activation in mouse embryos. Development *148*. 10.1242/dev.199426.